

Circulation: Arrhythmia and Electrophysiology

ORIGINAL ARTICLE



High Burden of Premature Ventricular Contractions Upregulates Transcriptional Markers of Inflammation and Promotes Adverse Cardiac Remodeling Linked to Cardiomyopathy

J.M.L. Medina-Contreras, PhD*; Jaime Balderas-Villalobos PhD*; Jose Gomez-Arroyo MD, PhD; Janée Hayles, MS; Karoly Kaszala MD, PhD; Alex Y. Tan MD; Montserrat Samsó PhD; Jose F. Huizar MD; Jose M. Eltit PhD

BACKGROUND: Premature ventricular contractions (PVCs) are the most prevalent ventricular arrhythmia in adults. High PVC burden can lead to left ventricular systolic dysfunction, eccentric hypertrophy, and an increased risk of heart failure and sudden cardiac death. Inadequate angiogenesis is a key determinant in the transition from adaptive to maladaptive cardiac hypertrophy, and fibrosis is a risk factor for arrhythmia and sudden cardiac death. We quantitatively assessed structural remodeling and transcriptional alterations in PVC-induced cardiomyopathy (PVC-CM).

METHODS: Animals were implanted with modified pacemakers to deliver bigeminal PVCs (200–220 ms coupling interval) for 12 weeks. Collagen deposition and interstitial ultrastructure of left ventricular samples were analyzed using light and transmission electron microscopy, respectively. Pericytes, fibroblasts, myocytes, smooth muscle, and endothelial cells were imaged using confocal microscopy, quantified with an artificial intelligence-based segmentation analysis, and compared using hierarchical statistics. Transcriptional changes were assessed via RNAseq, and protein expression was assessed using western blot.

RESULTS: Although cardiomyocytes hypertrophied in PVC-CM, capillary rarefaction was overcome by an increase in the capillary-to-myocyte ratio. Additionally, thicker blood vessels were more abundant in PVC-CM. Fibroblast-to-myocyte ratio more than doubled, interstitial collagen fibers increased, and interstitial space thickened in PVC-CM. Transcripts involved in interstitial remodeling, inflammatory response, and alarmins were strongly elevated in PVC-CM, showing enrichment of NF- κ B (nuclear factor kappa-light-chain-enhancer of activated B cells) transcriptional signature. These results coincide with elevated levels of the proinflammatory cytokine IL (interleukin)-1 β , the inflammasome component NLRP3 (nucleotide-binding domain, leucine-rich repeat family, pyrin domain containing 3), and increased expression of NF- κ B p65 (RelA).

CONCLUSIONS: Although the angiogenic response meets the metabolic demands of cardiac hypertrophy, upregulated markers of inflammation and cardiomyopathy linked to reactive fibrosis collectively represent an adverse left ventricular remodeling in PVC-CM that could provide the substrate for heart failure, arrhythmias, and sudden cardiac death in PVC-CM.

GRAPHIC ABSTRACT: A graphic abstract is available for this article.

Key Words: angiogenesis ■ cytokine ■ fibroblasts ■ heart failure ■ inflammation

Premature ventricular contractions (PVCs) are the most prevalent ventricular arrhythmia in adults and often affect the elderly population.^{1,2} The sporadic

occurrence of PVCs is believed to be benign; however, frequent PVCs have been recognized as a cause of heart failure and left ventricular (LV) systolic dysfunction known

Correspondence to: Jose M. Eltit, PhD, Department of Cellular, Molecular and Genetic Medicine, School of Medicine, Virginia Commonwealth University, 1101 E Marshall St, 3-038H, Richmond, VA 23298. Email jose.eltit@vcuhealth.org

*J.M.L. Medina-Contreras and J. Balderas-Villalobos contributed equally.

Supplemental Material is available at <https://www.ahajournals.org/doi/suppl/10.1161/CIRCEP.125.014195>.

For Sources of Funding and Disclosures, see page 46.

© 2026 American Heart Association, Inc.

Circulation: Arrhythmia and Electrophysiology is available at www.ahajournals.org/journal/circep

WHAT IS KNOWN?

- A high burden of premature ventricular contractions (PVC) can lead to ventricular dysfunction, a condition known as PVC-induced cardiomyopathy (PVC-CM).
- PVC-CM is associated with heart failure and likely increased mortality and sudden cardiac death.
- Animal models of PVC-CM show cardiac hypertrophy and fibrosis. Cardiac fibrosis is a well-known substrate for heart failure and sudden cardiac death.

WHAT THE STUDY ADDS

- PVC-CM is associated with cardiomyocyte hypertrophy without capillary rarefaction, supported by a proportional increase in the capillary-to-myocyte ratio.
- The fibroblast-to-myocyte ratio more than doubled in PVC-CM, accompanied by increased interstitial collagen deposition and thickening of the interstitial space.
- Together with fibrosis, an inflammatory response contributes to the adverse remodeling observed in PVC-CM.

Nonstandard Abbreviations and Acronyms

eNOS	endothelial nitric oxide synthase
IB4	isolectin B4
IL-1β	interleukin 1 β
LV	left ventricle
NF-κB	nuclear factor kappa-light-chain-enhancer of activated B cell
PVC-CM	PVC-induced cardiomyopathy
PVC	premature ventricular contraction
VEGF	vascular endothelial growth factor
VIM	vimentin
WGA	wheat germ agglutinin
αSMA	α -smooth muscle actin

as PVC-induced cardiomyopathy (PVC-CM).^{2,3} Importantly, LV dysfunction together with high PVC burden has been associated with an increased risk of mortality, ventricular arrhythmias, and sudden cardiac death.^{4–6}

PVCs are ectopic ventricular beats that originate in ventricular tissue and result in dyssynchronous contraction due to slow myocardial activation. High-burden PVCs progressively lead to cardiac remodeling characterized by decreased LV contractility (systolic dysfunction), electromechanical latency, and eventually, eccentric hypertrophy and LV dilatation.^{7,8} Whereas large animal models have been instrumental to systematically demonstrate that frequent PVCs cause PVC-CM,^{9,10} the mechanisms whereby frequent PVCs increase mortality are poorly understood.^{4,5}

Structurally, PVC-CM hearts show eccentric hypertrophy characterized by increased LV mass index with decreased relative wall thickness.⁸ Additionally, frequent PVCs also induce interstitial (or diffuse) fibrosis in the ventricle.^{10–12} LV hypertrophic responses are associated with neo-angiogenesis, likely as a compensatory mechanism to support the increased energy demand. Indeed, inadequate angiogenesis is a key step in the transition from an adaptive to maladaptive (or decompensated) cardiac hypertrophy.^{13–17} Here, we extend the characterization to samples obtained from the same cohorts of canines subjected to high-burden PVCs and sham procedures previously described in Balderas et al.¹⁸ We quantitatively evaluate fibrotic and angiogenic responses, along with underlying transcriptional adaptations.

METHODS

Data Availability Statement

The data supporting this study's findings are available from the corresponding author on reasonable request.

Animal Model

This study conforms to the Guide for the Care and Use of Laboratory Animals approved by the Institutional Animal Care and Use Committee at the Central Virginia HCS. Female mongrel canines (>10 months old, ≈21 kg) were implanted with a modified dual-chamber epicardial pacemaker via left thoracotomy.⁹ Pacemaker implantation was performed under general anesthesia using acepromazine (0.5–2 mg/kg, PO) and methohexitol sodium (6–10 mg/kg, IV) for induction, and inhaled isoflurane (2%–3%, endotracheal intubation) for maintenance throughout the procedure as previously described.⁹ Echocardiograms were performed at baseline and every 4 weeks as previously described.⁹ Penicillin G 900 000 units IM were administered 12 hours before surgery. Postoperatively, buprenorphine (0.1–0.2 mg/kg, IM) twice daily for 3 days was administered for pain control. After a 2-week surgical recovery, animals were randomized into 2 groups: (1) PVC-CM group, receiving bigeminal PVCs (50% burden) with a 200 to 220 ms coupling interval for 12 weeks, and (2) sham group, where PVCs were not enabled. Echocardiographic recordings were obtained at baseline and at 12 weeks of chronic PVCs to evaluate the development of cardiomyopathy. The tissue samples used in this study were obtained from the same experimental animal groups described in our previous publication.¹⁸ Euthanasia was performed at week 12, via exsanguination during the final left thoracotomy surgery under general anesthesia. The harvested heart was immediately rinsed with ice-cold PBS, which was injected directly through the left main coronary artery to remove blood. Segments of the anterior LV were (1) snap-frozen in liquid nitrogen for biochemical analysis, (2) fixed in 10% neutral buffered formalin for optical microscopy, and (3) perfused first with 2 mmol/L EGTA and 16 mmol/L KCl in PBS, followed by fixation in 4% glutaraldehyde, 0.1M cacodylate, pH 7.4, for transmission electron microscopy. Freshly fixed tissue samples were used in immunostaining experiments to prevent damage caused by freezing. However, due to the limited availability of

fresh samples as the project progressed, the number of animals used for different molecular markers varied.

RNA Sequencing of LV Samples

Snap-frozen myocardial tissue from randomly selected regions of the LV free wall was used for RNA extraction. Total RNA was isolated using the RNeasy kit (Qiagen, MD) to generate 14 ribo-depleted, paired-end, 75 base-pair stranded RNA libraries (6 samples from sham animals and 8 from PVC-CM animals). Samples were sequenced using an Illumina NextSeq sequencing platform. Reads were pseudo-aligned and quantified using an index transcriptome version of the CanFam3.1 dog genome assembly (GCA_000002285.2) using Kallisto with standard settings.¹⁹ Transcript-level abundance estimates were imported and summarized as a counts matrix using tximport.²⁰ Gene-level exploratory analysis and differential gene expression were performed using DESeq-2 R with standard settings, setting a Benjamini and Hochberg false discovery rate of <0.1.²¹ Data have been deposited in the Gene Expression Omnibus public repository under accession number GSE296225.

Western Blotting

LV free wall frozen samples were pulverized in a mortar under liquid nitrogen, and proteins were extracted using specific buffers described in the [Supplemental Material](#). Proteins were separated using polyacrylamide gel electrophoresis, then transferred to PVDF membranes, incubated with primary and secondary antibodies, and developed using an enhanced chemiluminescent assay. Primary antibodies used in this study are described in [Table S1](#).

Immunostaining

Tissue slices (40 µm thick; obtained with a Leica vibratome V1 1000S) from 10% neutral buffered formalin fixed LV free wall were subjected to antigen retrieval (abcam, ab93684), then incubated with primary antibodies or lectins described in [Table S2](#). This was followed by appropriate secondary antibody and DAPI incubation, washed with PBS, placed on slides, and mounted using ProLong Gold (Invitrogen) media. Cardiac tissue was examined using confocal laser scanning microscopy (Zeiss LSM 700). Colocalization and artificial intelligence-powered analyses (AIVIA software) are described in the [Supplemental Material](#).

Collagen Determinations Using Sirius Red Fast Green Staining In Situ

The 10% neutral buffered formalin fixed tissue was paraffin embedded, sectioned (10 µm thick, Reichert-Jung 820 II, rotary microtome), rehydrated, and stained with Sirius Red/Fast Green.²² Micrographs were acquired at 20X using a Carl Zeiss microscope (Axio Imager Z2) equipped with a color camera. Image analysis is described in the [Supplemental Material](#).

Transmission Electron Microscopy

Samples were fixed in 4% glutaraldehyde, stained using 2% osmium tetroxide and saturated uranyl acetate, and infiltrated with Embed 812 resin as previously described.¹⁸ Images were acquired on a Tecnai F20 or a Jeol JEM-1230 transmission

electron microscope, both equipped with a Gatan UltraScan 4K×4K CCD camera.

Statistical Analysis

Data distribution of Western blots (single measure per animal) was determined using the Kolmogorov-Smirnov test, and an unpaired *t* test or Mann-Whitney *U* test was used to compare differences between groups for parametric or nonparametric distributions, respectively.

When multiple measurements were collected per animal (eg, AIVIA analysis and *in situ* Sirius red/fast green collagen determination) nested *t* test, a hierarchical statistical method, was used for comparison of the data.^{23,24} Hierarchical statistics (nested *t* test) account for the variability both within and between subjects.^{23,24} Because repeated measurements from the same animal are not independent, applying a standard *t* test is inappropriate. The nested *t* test, implemented as a mixed-effects model, accounts for the hierarchical structure of the data by modeling technical replicates as nested within animals, reducing the risk of type I error (false positives).²⁴ This test is currently implemented in recent versions of GraphPad Prism. The number of animals (N) and the number of technical replicas (ie, no. of images) studied in each experiment are indicated in the corresponding figure or in the table. In addition, for hierarchical statistical analyses, data were represented using a box and whiskers plot along with individual values.

The threshold for the significant difference was *P*<0.05. GraphPad Prism 9.3.1 was used as a statistical software resource.

RESULTS

Cardiomyocyte Hypertrophy

Previously, we reported the development of eccentric hypertrophy⁸ and an increase in cardiomyocyte size.¹⁸ The cohorts of animals used in the latter work are the same as those used here, where the echocardiographic results showed $44.36 \pm 5.31\%$ versus $61.91 \pm 5.61\%^{***}$ LV ejection fraction, in the 12-week-PVC-CM and sham cohort, respectively (Šídák multiple comparisons test, $****P<0.0001$).¹⁸ Analysis of *in situ* cross-sectional myocyte size in PVC-CM samples shows a 38% larger surface area than in shams (20 287 and 21 070 myocytes analyzed in the PVC-CM and sham groups, respectively, *P*<0.001, nested *t* test; see [Table 1](#)).

Interstitial and Perivascular Fibrosis

Fibrosis was assessed by staining collagen *in situ* and followed by visualization under light microscopy. In longitudinal sections, the PVC-CM group showed a 4-fold increase in fibrosis compared with the sham group ([Figure 1A; Table 1](#)). In cross-sections, the PVC-CM group showed a 3.8-fold increase, while perivascular fibrosis increased by 2.2-fold ([Figure 1A; Table 1](#)). Cross-sections were also studied under the electron microscope to visualize ultrastructural changes of the interstitial space.

Table 1. Quantification of Cellular Composition of LV Tissue

	Sham		PVC		
	Mean±SD	No. of images (No. of animals)	Mean±SD	No. of images (No. of animals)	Nested t test, P value
Myocyte cross-sectional area, μm^2 *	237±49.3	94 (7)	328±94.3	128 (6)	0.001
% of fibrosis (longitudinal)	2.1±1.0	69 (6)	8.5±5.0	83 (6)	0.002
% of fibrosis (cross-section)	2.1±1.6	62 (6)	7.8±6.1	77 (6)	0.026
% of fibrosis (perivascular)	7.6±4.3	39 (6)	17.0±9.9	52 (6)	0.0001
Pericyte density (number/mm ² , cross-section)	3301±1092	40 (5)	3020±809	57 (5)	0.489
Pericyte number/cardiomyocyte (cross-section)	1.44±0.48	40 (5)	1.87±0.60	57 (5)	0.115
Blood vessel† sectional area, μm^2 (cross-section)	46.5±42.4	36 (5)	86.2±65.5	54 (5)	0.047
Blood vessel† density (number/mm ² , cross-section)	31.2±43.0	36 (5)	188.3±116.5	54 (5)	0.017
Area covered by blood vessel‡ (%), cross-section)	0.17±0.30	36 (5)	1.48±0.92	54 (5)	0.004
Fibroblast density (number/mm ² , cross-section)	1149±379	62 (4)	1444±434	59 (4)	0.077
Fibroblast number/cardiomyocyte (cross-section)	0.53±0.30	62 (4)	1.15±0.54	59 (4)	0.010
Capillary sectional area, μm^2 (cross-section)	17.1±3.3	63 (4)	25.7±3.9	88 (4)	0.004
Capillary density (number/mm ² , cross-section)	2857±432	63 (4)	2681±456	88 (4)	0.362
Capillary number/cardiomyocyte (cross-section)	1.36±0.18	63 (4)	1.62±0.18	88 (4)	0.035
Area covered by capillaries (%), cross-section)	4.83±1.2	63 (4)	6.86±1.68	88 (4)	0.033

LV indicates left ventricle; and PVC, premature ventricular contraction.

*Data from Balderas-Villalobos et al¹⁸ plus additional new determinations.

†Blood vessels excluding capillaries.

Cardiomyocytes and capillaries (endothelial cells) were clearly identified in the transmission electron microscopy images of fixed LV samples (Figure 1B). In Figure 1B, the interstitial space (highlighted in yellow) is enlarged in the PVC-CM group compared with the sham group, consistent with the increased interstitial fibrosis observed in PVC-CM by optical microscopy (Figure 1A).

Identification of Cell Types and Vascular Structures in LV Tissue

To better characterize the cellular adaptations occurring in PVC-CM, a set of 4 markers was used: SMA (-smooth muscle actin), VIM (vimentin), IB4 (isolectin B4), and DAPI. SMA immunostaining unveiled abundant pericytes, thin and long cells in the interstitial space of the myocardium,^{25–27} depicted in red (Figure 2A). In addition, the anti-SMA antibody recognized smooth muscle cells forming the tunica media of blood vessels (see cross-section in Figure 2A). Conversely, IB4 showed a selective stain for endothelial cells (green cells in Figure 2A), which constitute both the capillaries and the tunica intima of larger blood vessels (Figure 2A).^{25–28} VIM immunostaining unveiled fibroblasts^{29,30} in the interstitium (white in Figure 2A) and labeled endothelial cells in the tunica intima of large blood vessels (Figure 2A cross-section), but was undetectable in endothelial cells forming capillaries.

Confocal images showed a clear increase in blood vessels in PVC-CM versus sham for both cross- and longitudinal sections (Figure 2B). Additionally, the very

well-organized interaction between pericytes and capillary endothelial cells was clearly observed in longitudinal sections in both groups (Figure 2B merge).

Myofibroblasts (as fibroblasts) are involved in collagen deposition, but, in contrast to fibroblasts, they are particularly important in scar compaction during replacement fibrosis.³¹ It is well known that fibroblast to myofibroblast differentiation requires an increase in expression of the contractile protein SMA.^{32,33} Myofibroblast presence, thus, may be captured by the colocalization of SMA and VIM staining.³⁴ The SMA⁺ and VIM⁺ cells present in the interstitium produced distinctive staining patterns with apparent low colocalization (Figure S1; Table 2). Because SMA and VIM can also colocalize in the boundary between the tunica media and the intima of blood vessels, the colocalization parameters between SMA and VIM staining were determined, including and omitting blood vessels. Persson and Mander correlation coefficients³⁵ did not show significant statistical differences between the sham and PVC-CM groups (Table 2), and any increase was nullified when blood vessels were omitted from the analysis. This suggests that SMA is not overexpressed in VIM⁺ fibroblasts and that there is limited differentiation toward a myofibroblast phenotype in the PVC-CM group.

Morphometric Assessment of Pericytes and Vasculature

As shown in Figure 2A, SMA was expressed mainly in pericytes and vascular smooth muscle cells with

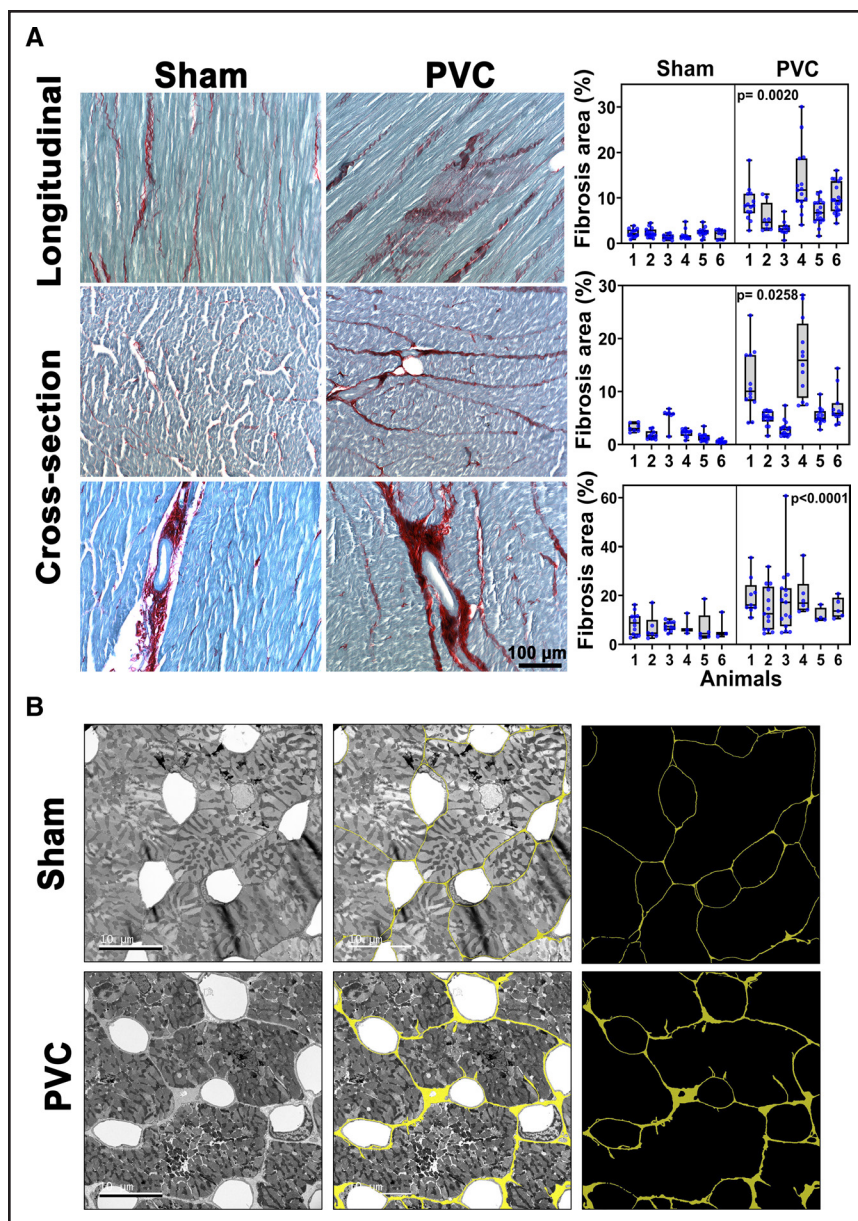


Figure 1. Fibrosis is elevated in premature ventricular contraction-induced cardiomyopathy (PVC-CM).

A, Representative images of left ventricular (LV) free wall samples stained with Sirius red/fast green to detect fibrotic depositions. Images were obtained from longitudinal (**upper**) and cross-sections (**middle** and **lower**) from sham and PVC-CM animals. The red staining reveals interstitial fibrosis (**upper** and **middle**) and fibrosis in perivascular regions (**lower**). Percentual area covered by collagen deposits was quantified; data from each animal are represented using a box plot (interquartile range and median) and whisker plot (min and max values), and data from each image are represented by blue dots (right graphs and Table 1). Both groups are compared using hierarchical statistics (nested *t* test), and *P* values are shown in each graph. **B**, Ultrastructural analysis using transmission electron microscopy (TEM). Representative TEM micrographs of LV thin cross-sections from sham and PVC-CM groups (**left**). The AIVIA software was used to highlight the interstitial space shown in yellow (**merged** in the **middle**); for comparison purposes, the interstitial space is shown alone (**right**).

apparent lack of expression in VIM⁺ fibroblasts. First, Western blot was used to quantify SMA in whole LV tissue lysates, the PVC-CM group showed a 64% increase in expression compared with the sham group ($P<0.0001$ *t* test, $n=6$ animals per group, Figure 3A). Western blot shows the total expression of the protein, regardless of the cell type in which it is expressed. Then, to better estimate the subpopulation of cells responsible for the increase in SMA, we performed quantitative morphometric determinations of confocal images stained with anti-SMA antibody. In cross sections, the pattern was split into 2: the SMA⁺ pericytes and the distinctive ring-shaped tunica media (smooth muscle layer) of blood vessels (Figure 3B). In the same confocal image, myocytes were identified, and their total number was quantified using WGA (wheat germ agglutinin) staining and

the AIVIA software, respectively (Figure 3B). This procedure allowed us to quantify the number of pericytes, the number of blood vessels (excluding capillaries), and the total number of myocytes per image. The density of pericytes (pericyte/mm²) was similar in PVC-CM and the sham group (Table 1; Figure 3C; $P=0.489$, nested *t* test). After accounting for the hypertrophy-induced increase in myocyte size in the PVC-CM group¹⁸ (Table 1), the calculated pericyte-to-cardiomyocyte ratio revealed a trend of ≈30% more pericytes per myocyte in the PVC-CM group, which was not statistically significant (Table 1; Figure 3C, $P=0.115$, nested *t* test). The PVC-CM group showed blood vessels (excluding capillaries) with 86% larger sectional area than the sham group (Table 1; Figure 3C; $P=0.047$ nested *t* test). In addition, the density of blood vessels (number per mm²) and the percentage

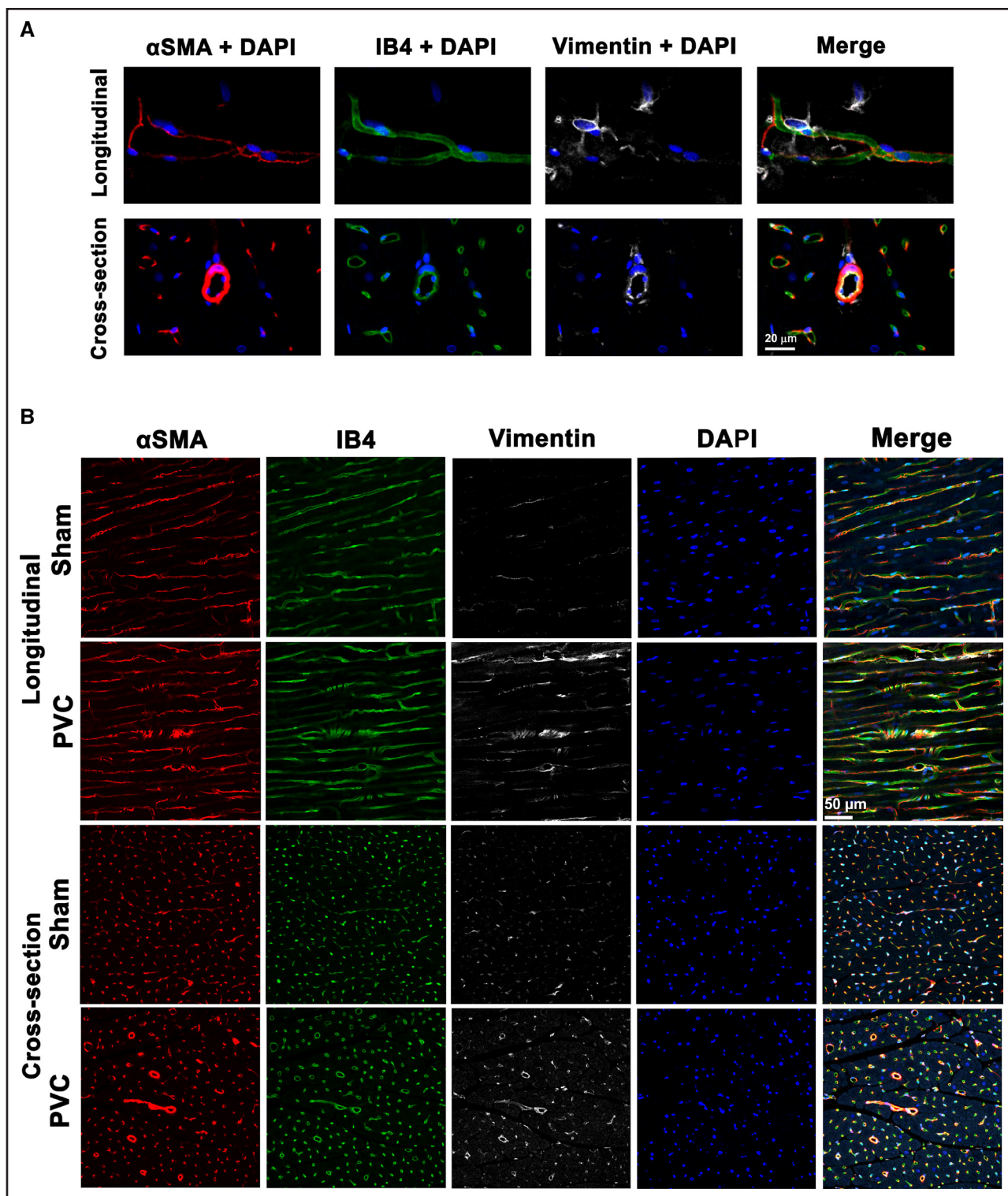


Figure 2. Identification of cells and structures in cardiac tissue using different cellular type markers.

A, Representative images showing formalin-fixed left ventricular (LV) free wall tissue samples costained using anti- α SMA (α -smooth muscle actin; red), anti-VIM (VIM, white), IB4 (isolectin B4, green), and DAPI as counterstain (blue). In our experimental conditions, each marker recognized distinctive cell types and structures that were then quantified using the AIVIA software. In the longitudinal image (**upper**), α SMA⁺ cells show a structure compatible with pericytes, IB4⁺ cells are structurally compatible with capillary endothelial cells, and VIM⁺ cells identify fibroblasts. Cross-section (**lower**) shows that anti- α SMA antibody stains the tunica media of blood vessels; IB4 stains capillaries and the tunica intima of blood vessels, and the anti-VIMENTIN antibody stains the tunica intima of blood vessels and fibroblasts. **B**, Representative images showing formalin-fixed LV free wall tissue samples of the 2 experimental groups costained with anti- α SMA, IB4, anti-VIM, and DAPI as counterstain.

Table 2. Colocalization Analysis of Vimentin and α -Smooth Muscle Actin in Costained Tissue (mean \pm SD)

	No. of animals	No. of images	Pearson R	M1* norm	M2* norm	%pixels
Whole tissue						
Sham	3	41	-0.082 ± 0.144	0.367 ± 0.146	0.122 ± 0.064	0.31 ± 0.26
PVC	3	71	-0.104 ± 0.089	0.484 ± 0.103	0.212 ± 0.098	0.90 ± 0.55
		Nested t test	$P=0.646$	$P=0.257$	$P=0.204$	$P=0.065$
Removing blood vessels						
Sham	3	41	-0.140 ± 0.080	0.294 ± 0.103	0.069 ± 0.053	0.10 ± 0.07
PVC	3	71	-0.158 ± 0.085	0.311 ± 0.084	0.096 ± 0.054	0.18 ± 0.10
		Nested t test	$P=0.424$	$P=0.816$	$P=0.427$	$P=1.052$

PVC indicates premature ventricular contraction.

*Mander correlation coefficients.

area covered by them were 6-fold ($P=0.017$, nested *t* test) and 8.7-fold ($P=0.004$, nested *t* test) larger, respectively, in PVC-CM when compared with the sham group (Table 1; Figure 3C).

Morphometric Analysis of Fibroblasts

VIM was strongly elevated when assessed using Western blot in 4 out of 6 PVC-CM samples, showing a 139% increase compared with the sham group. However, this trend was not statistically significant, $P=0.085$ *t* test, due to high data dispersion (Figure 4A).^{36,37}

The AIVIA software was trained to identify the staining pattern consistent with VIM⁺ fibroblasts (ie, excluding the blood vessel staining pattern) and the total number of myocytes in the corresponding WGA channel from the same confocal image (Figure 4B). The density of fibroblasts (fibroblasts/mm²) was 26% larger in PVC-CM samples than in sham, which almost reached statistical significance (Table 1; Figure 4C; $P=0.077$, nested *t* test). Importantly, the PVC-CM group doubled (2.2-fold) the number of fibroblasts compared with the sham group when adjusted per number of myocytes (Table 1; Figure 4C; $P=0.010$, nested *t* test), suggesting the active proliferation of fibroblasts in PVC-CM.

Morphometric Analysis of Capillaries

Capillary rarefaction was studied since it is a key characteristic of maladaptive hypertrophy. Western blot analysis of whole tissue samples was performed, measuring proteins involved in the function and remodeling of capillaries. Both, the eNOS (endothelial nitric oxide synthase, a key protein involved in the generation of NO)³⁸ and the VEGF-B (vascular endothelial growth factor-B, a strong angiogenic growth factor)³⁹ were elevated in the PVC-CM LV samples compared with the sham group (21% increase, $P<0.036$, and 34% increase $P<0.003$, respectively, *t* test; Figure 5A).

The AIVIA software was trained to identify endothelial cells (IB4⁺) forming capillaries but reject the ones

forming the intima of blood vessels (Figure 5B). Additionally, WGA staining was used to compute the total number of myocytes (Figure 5B). The morphometric assessment showed that the PVC-CM group had capillaries with 50% larger cross-sectional area than the sham group (Table 1; Figure 5C; $P=0.004$ nested *t* test). The density of capillaries (number of capillaries/mm²) was not different between the 2 experimental groups (Table 1; Figure 5C; $P=0.362$, nested *t* test), but the PVC-CM group had 19% more capillaries per myocyte than the sham group (Table 1; Figure 5C; $P=0.035$, nested *t* test). In addition, the area covered by capillaries in the cross-section images was 42% larger in PVC-CM versus the sham group (Table 1; Figure 5C; $P=0.033$ nested *t* test).

Figure 6 (left panels) shows transmission electron microscopy images from representative sham and PVC-CM LV samples depicting multiple contiguous capillaries with different sizes and interstitial cells (pericytes) interconnecting capillaries in the PVC-CM group (arrows in Figure 6), an arrangement rarely observed in sham micrographs. In the corresponding confocal cross-section images (Figure 6 right panels), several examples of SMA⁺ cells (pericytes, displayed in red) were interacting either with single capillaries (in green) or connecting pairs of capillaries showing a similar structural arrangement to that observed in the PVC-CM transmission electron microscopy image. In contrast, capillaries interconnected by pericytes are less frequent in sham samples (Figure 6 right panels).

RNA Seq Analysis of LV Samples

Bulk RNA sequencing was performed to uncover transcriptional changes driving cardiac adaptations observed in PVC-CM. Compared with sham, PVC-CM had a total of 646 (2.9%) and 470 (2.1%) genes upregulated or downregulated, respectively. The heatmap in Figure 7A displays the top 50 upregulated genes. Gene set enrichment analysis of the top 50 upregulated genes revealed significant associations with biological processes related

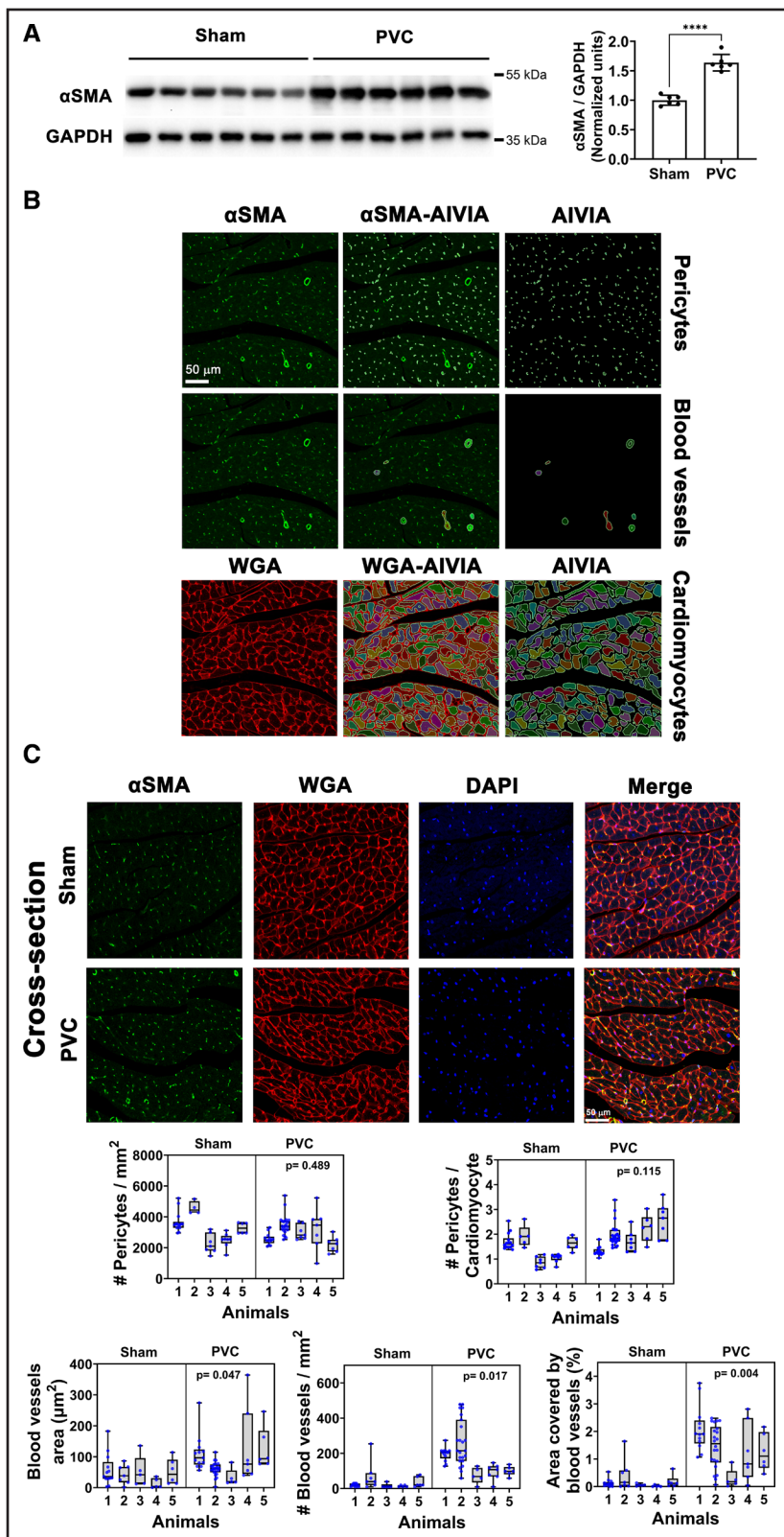


Figure 3. Protein expression and morphometric analysis of αSMA (α-smooth muscle actin) revealed pericytes and blood vessels in left ventricular (LV) cardiac tissue.

A, Western blot analysis shows an increase in αSMA expression in premature ventricular contraction-induced cardiomyopathy (PVC-CM) vs sham ($P < 0.0001$ *t* test, $n=6$ animals per group, bars represent mean \pm SD).

B, Representative LV cross-sections costained with anti-αSMA antibody (green) and WGA (wheat germ agglutinin)-AF633 (red; **left**). Artificial intelligence-based (AIVIA) recognition and segmentation of αSMA⁺ cells (pericytes) and blood vessels, and WGA-stained cardiomyocytes overlaid with the original image (**middle**). AIVIA generated regions of interest (ROIs) corresponding to pericytes, blood vessels, and cardiomyocytes (**right**). **C**, Representative formalin-fixed LV cross-sections costained using anti-αSMA (green), WGA-AF633 (red), and DAPI (blue) in sham and PVC-CM LV free wall samples. The identified ROIs were used to calculate the number of pericytes, the number and area of blood vessels, and the number of myocytes (WGA) on each image. AIVIA results are plotted and analyzed using hierarchical statistics (nested *t* test). The density (number of pericytes per mm²) and number of pericytes per cardiomyocyte were quantified for several images per animal. In total 13 529 vs 17 641 pericytes were analyzed for sham vs PVC, respectively. The unitary area of blood vessels (μm²), density (number of blood vessels per mm²), and the percentage of area covered by blood vessels were also quantified using the artificial intelligence-based software. The total number of blood vessels analyzed was 36 vs 54 in the sham vs PVC-CM group, respectively. Several micrographs were quantified per animal (see Table 1). Each point in the graphs represents the mean value per micrograph, and the data are displayed as a box plot (interquartile range and median) and whisker plot (min and max values).

to proteolysis, neutrophil chemotaxis, immune response, and extracellular matrix organization (Figure 7B). The transcriptional signature also showed enrichment for transcriptional regulatory networks associated with

nuclear factor kappa-light-chain-enhancer of activated B cells (NF-κB) or RELA (which encodes a subunit p65 of NF-κB), as determined by transcriptional regulatory relationship analysis (using TRRUST5 software; Figure 7C).

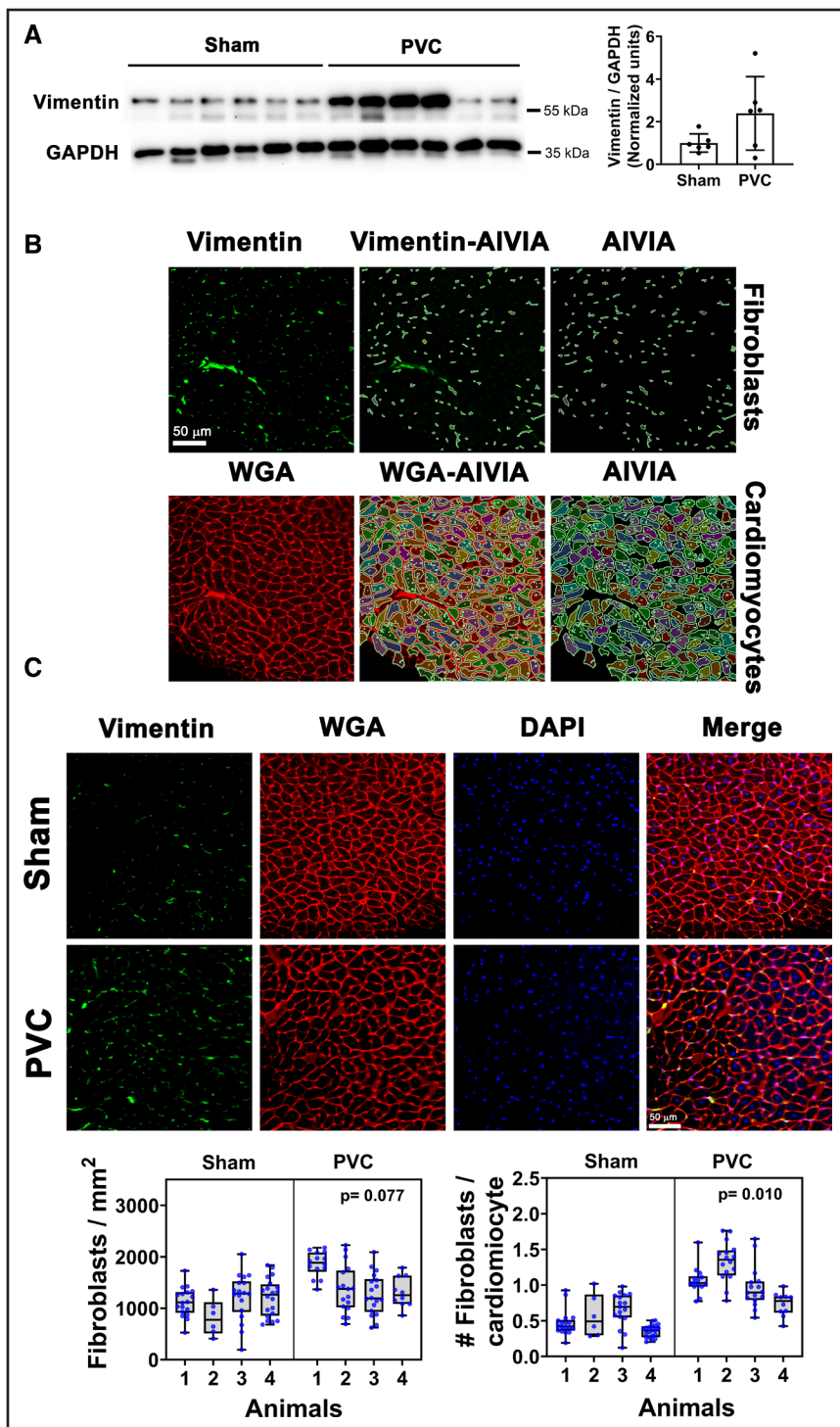


Figure 4. Frequent premature ventricular contractions (PVCs) increase fibroblast content.

A, Western blot study was used to measure vimentin expression in the left ventricular (LV) tissue in PVC-induced cardiomyopathy (PVC-CM) with respect to sham ($P=0.085$ *t* test, $n=6$ animals per condition, bars represent mean \pm SD).

B, Original representative LV cross-sections costained with anti-vimentin antibody (green) and WGA (wheat germ agglutinin)-AF633 (red; **left**). AI-powered image segmentation merged with the representative image (middle panels). The segmentation result showed fibroblasts and cardiomyocytes, while blood vessel structures were rejected (**right**).

C, Representative LV cross-sections costained using anti-vimentin (green), WGA-AF633 (red), and DAPI (blue) in sham and PVC-CM samples. The ROIs identified were used to calculate the number of fibroblasts and the number of myocytes on each image. Results from the AIVIA software were plotted and analyzed using hierarchical statistics (nested *t* test). Density (number of fibroblasts per mm^2) and number of fibroblasts per cardiomyocyte were quantified for several images. The number of fibroblasts analyzed was 7305 and 7407 for the sham and PVC-CM group, respectively. Each point in the graphs represents the mean value per micrograph, and the data is displayed as a box plot (interquartile range and median) and whisker plot (min and max values).

The top 5 upregulated genes in PVC-CM were metalloproteinases MMP (matrix metalloproteinase) 8 (31-fold increase and adjusted *P* value 1.67E-9), MMP9 (28-fold increase and adj *P* value 3.58×10^{-4}), and MMP3 (6-fold increase and adj *P* value 0.007; Figure 7D). Other metalloproteinases, such as ADAMTS (a disintegrin and metalloproteinase with thrombospondin motifs) 9 and ADAMTS4, are also upregulated, as well as the MMP inhibitor TIMP (tissue inhibitor of metalloproteinases)

1 (Figure 7A). We identified upregulation of numerous genes linked to macrophage activation, immune cell recruitment, and cytokine signaling/production, including CCL (C-C motif chemokine ligand) 20 (13-fold increase and adj *P* value, 0.045), CSF (colony-stimulating factor) 3 (13-fold increase and adj *P* value, 0.008), and PTX (pentraxin) 3 (9-fold increase and adj *P* value, 2.25×10^{-8} ; Figure 7D). Additionally, SELE (E-selectin), CXCR (C-X-C motif chemokine receptor) 1, CXCR2,

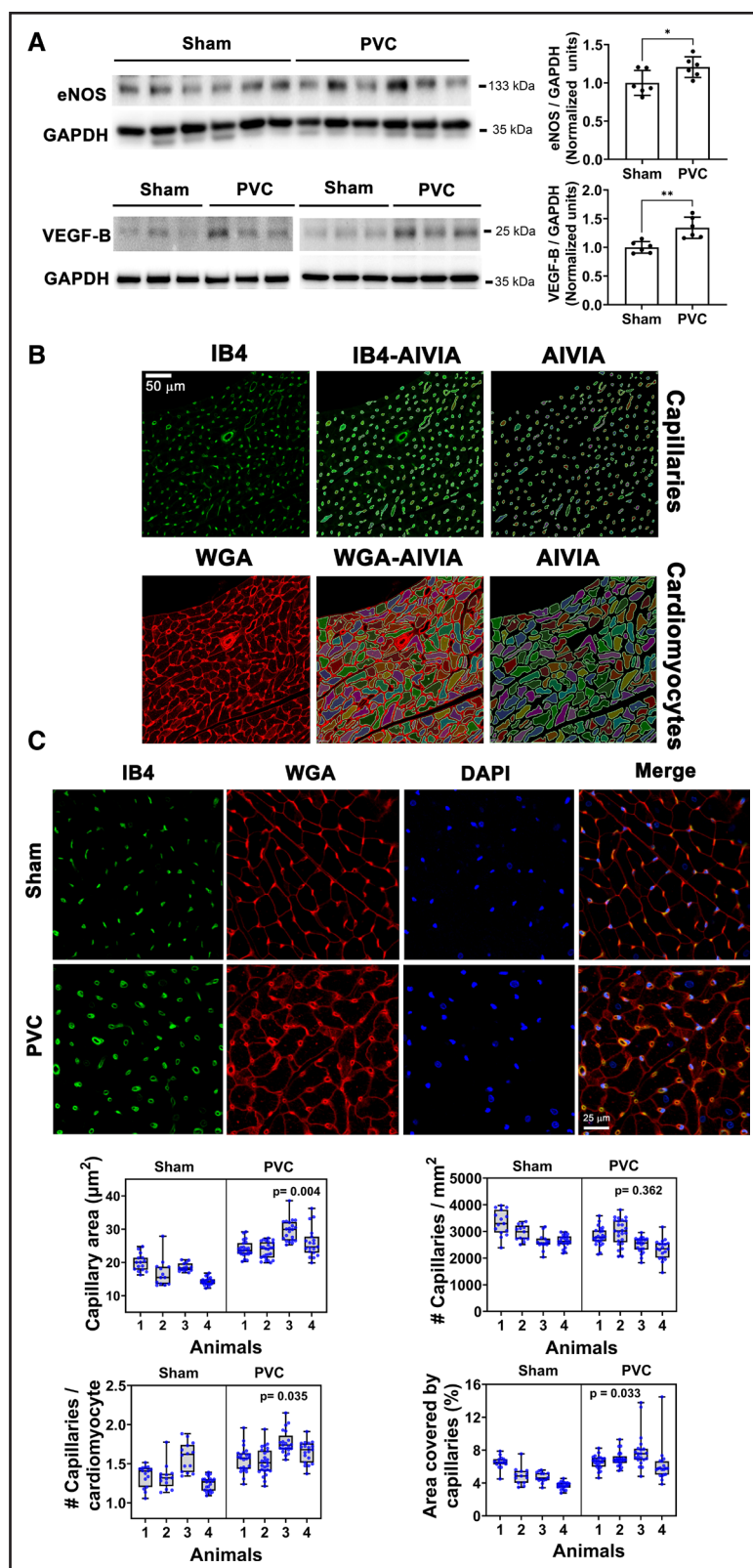


Figure 5. Frequent premature ventricular contractions (PVCs) promote an angiogenic response.

A, Western blot analysis indicates increased expression of eNOS (endothelial nitric oxide synthase; $P<0.036$ t test, $n=6$ animals per condition) and VEGF (vascular endothelial growth factor)-B ($P<0.003$ t test, $n=6$ animals per condition), bars represent mean \pm SD. **B**, Original representative left ventricular (LV) cross-sections costained with IB4-AF488 (green) and WGA (wheat germ agglutinin)-AF633 (red; **left**). AI-based detection of capillaries and cardiomyocytes using the AI-powered AIVIA classifier merged with the original images (**middle**). Capillaries and cardiomyocytes were recognized by the AI segmentation, while blood vessel structures were rejected (**right**). (*Continued*)

Figure 5 Continued. C, Representative LV cross-sections costained with IB4 (green), WGA-AF633 (red), and DAPI (blue) in sham and PVC-induced cardiomyopathy (PVC-CM). The recognized ROIs were used to calculate the number of capillaries, the area of capillaries, and the number of myocytes on each image. Results from AIVIA software were plotted and analyzed using hierarchical statistics (nested *t* test; Table 1). The unitary capillary area (μm^2), density (number of capillaries per mm^2), number of capillaries per cardiomyocyte, and the percentual area covered by capillaries were quantified for several images per animal. The number of capillaries analyzed was 18318 vs 24012 in the sham vs PVC-CM group, respectively. Several micrographs were analyzed per animal (data shown in Table 1), and the comparison between groups was performed using hierarchical statistical analysis (nested *t* test). Each point in the graphs represents the mean value per micrograph, and the data are displayed as a box plot (interquartile range and median) and whisker plot (min and max values).

ADGRE1 (adhesion G protein-coupled receptor E1), IL-6, SOCS3 (suppressor of cytokine signaling 3), and CCR1 (C-C chemokine receptor type 1) were all upregulated (Figure 7A), suggesting that inflammatory and fibrotic responses work together to sustain cardiac remodeling in PVC-CM. An additional set of genes of interest upregulated in the PVC-CM group were the S100 Ca^{2+} binding proteins S100A12 (12-fold increase and adj *P* value, 3.20×10^{-6}), S100A8 (10-fold increase and adj *P* value, 1.21×10^{-4}), and S100A9 (9-fold increase and adj *P* value, 6.89×10^{-5} ; Figure 7D). These genes (and their protein products) are key biomarkers for cardiac disease, playing a pivotal role in the inflammatory and fibrotic responses of the heart to pathological insults.

The amount of IL (interleukin) 1 β , an inflammatory cytokine mainly produced by macrophages associated with cardiac remodeling and fibrosis,^{36,37} showed a significant 69% increase in PVC-CM samples compared with the sham group (*P*=0.007, *t* test, Figure 7E). Similarly, NLRP3 (nucleotide-binding domain, leucine-rich repeat family, pyrin domain containing 3), also predominantly expressed in macrophages and a main component of the inflammasome,⁴⁰ was elevated in PVC-CM samples compared with sham (*P*=0.028, *t* test; Figure 7E). NF- κ B p65 (RelA) was elevated in PVC-CM samples compared with sham (*P*=0.017, *t* test, Figure 7E), while its phosphorylation was reduced at position Ser536 (*P*=0.018, *t* test, Figure 7E), consistent with the transcriptomic alterations placing NF- κ B p65 (RelA) as an important mediator of the observed transcriptional changes described above (Figure 7C).

DISCUSSION

Fibrosis in PVC-CM

Fibroblasts can exist in different states and levels of activation.^{32,33} A commonly used marker to assess fibroblast to myofibroblast differentiation is α SMA. This marker is associated with the expression of stress fibers, promoting migration and scar compaction.³¹ In fact, a high percentage of myofibroblasts are VIM⁺ and α SMA⁺ in models of replacement fibrosis such as myocardial infarction.³⁴ Although α SMA immunostaining was intended to identify myofibroblasts, it revealed patterns consistent with pericytes and smooth muscle of blood vessels (Figure 2A). In contrast, VIM staining within the interstitial cell population was convincingly selective for

fibroblasts in our LV samples (Figure 2A). Quantification of the VIM⁺ and α SMA⁺ co-localization signal (Figure S1; Table 2) showed no increase in PVC-CM compared with the sham group, suggesting that the myofibroblast population did not increase in PVC-CM. Yet, together with an increase in collagen content, we found a doubling of fibroblasts-to-myocyte ratio (VIM⁺ cells) in PVC-CM (Table 1), indicating that the number of fibroblasts is elevated in PVC-CM. These observations agree with other reports showing that myofibroblasts (α SMA⁺ fibroblasts) are usually not abundant in nonreplacement fibrosis,⁴¹ such as the reactive fibrosis observed in PVC-CM.

Reactive fibrosis usually responds to mechanical and neurohumoral stress. It affects cardiac contractility and promotes reentrant arrhythmias by changing electrophysiological tissue properties, including conduction velocity and ventricular activation patterns.^{42,43} Both local and regional myocardial fibrosis could have significant clinical implications as they are known predictors of ventricular arrhythmias and sudden cardiac death.^{4,44-49}

Angiogenesis and Eccentric Hypertrophy

An underlying function of activated fibroblasts is to provide mechanical and humoral support to endothelial cells during angiogenic responses.⁵⁰ Fibroblasts influence angiogenesis by secreting several angiogenic factors (eg, VEGF, FGF (fibroblast growth factor), angiopoietins, among others) and by modulating the stiffness of the extracellular matrix.⁵¹⁻⁵⁴ Our previous work showed elevated levels of VEGF-A¹⁸ and, as shown here, VEGF-B is similarly elevated in PVC-CM (Figure 5A). These factors have complementary functions in the angiogenic response.⁵⁵ VEGF-A is a potent master regulator of angiogenesis, mainly secreted by cardiomyocytes in the heart tissue,⁵⁶ which is important to initiate the formation of immature vessels by vasculogenesis and angiogenic sprouting.⁵⁷ In contrast, VEGF-B has a modulatory role in improving angiogenesis by promoting the survival of endothelial cells and multiple other cell types.³⁹ In addition, increased VEGFs have been associated with cardiac hypertrophy.^{58,59} eNOS, a protein abundant in endothelial cells but also expressed by cardiomyocytes, was also elevated in PVC-CM (Figure 5A), further supporting the presence of an angiogenic response in PVC-CM.

We previously reported an increase in LV mass index without a change in the relative wall thickness, which indicates eccentric hypertrophy.⁸ This finding was later

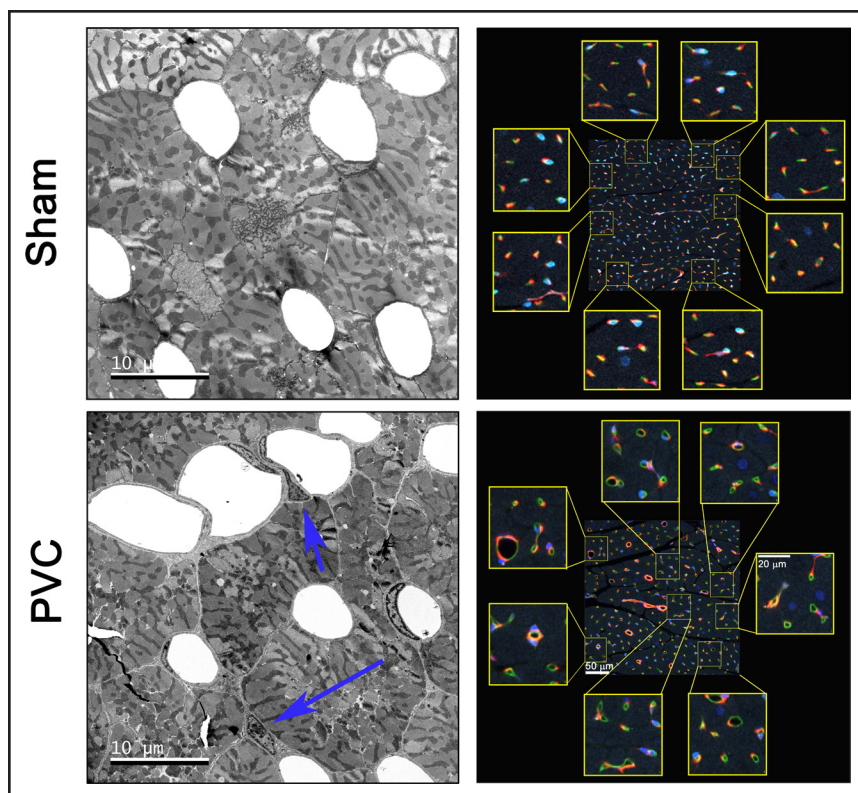


Figure 6. Transmission electron microscopy (TEM) and confocal microscopy reveal premature ventricular contraction-induced cardiomyopathy (PVC-CM) induced alterations in capillary and pericyte organization.

Left, Representative TEM micrographs showing contiguous capillaries with different calibers in PVC (arrangement rarely seen in the sham condition). The blue arrows indicate the presence of pericytes. **Right,** Representative left ventricular (LV) cross-section contained with IB4 (green; endothelial cells in capillaries and intima layer blood vessels), anti- α SMA (α -smooth muscle actin; red; pericytes and tunica media of blood vessels), anti-vimentin (white, fibroblasts), and DAPI (blue, nuclei); images taken from Figure 2B (merge). The enlarged quadrants show adjacent capillaries more abundant in the PVC condition, with some of them interconnected by pericytes similar to those in the TEM image.

confirmed by an increase in cross-sectional area of the ventricular myocytes in PVC-CM compared with the sham group *in situ*.¹⁸ At a tissue level, cardiomyocyte size increased in both width and length,¹⁸ together with an increase in cell capacitance measured in isolated ventricular myocytes,⁶⁰ findings that are consistent with eccentric hypertrophy in PVC-CM animals. It is well established that the transition from adaptive to decompensated cardiac hypertrophy largely evolves from capillary rarefaction.¹³ However, the density of capillaries remained unchanged in PVC-CM compared with the sham group (Table 1). Our capillary density values (Figure 5C; Table 1) are comparable to those reported in cardiac tissue by other groups.^{61,62} This lack of rarefaction in our PVC-CM model is achieved by increasing the capillary-to-myocyte ratio by 19% (Table 1), compensating for the volume “taken” by the hypertrophied myocytes. In addition, pericytes are supportive cells key for capillary function, including capillary lumen size regulation.^{63,64} Although the number of pericytes-to-myocyte ratio shows a tendency to increase, the absence of statistical significance (Table 1) may be attributed to instances where a single pericyte is shared between closely spaced capillaries, as observed in the zoomed panels of Figure 6. This phenomenon could suggest the formation of new capillaries in PVC-CM. Additionally, capillaries in the PVC-CM show a clear increase in their cross-sectional area, similar to what was described previously in a hypertrophy model induced by VEGF-B overexpression,⁶⁵ and

there is also a significant increase in the number of larger blood vessels. All these findings suggest that (1) vascular resistance should be reduced in the LV tissue, and blood perfusion should be favored in PVC-CM, (2) elevated angiogenesis and larger lumen of capillaries maintain appropriate blood supply to balance the metabolic demand of the hypertrophic phenotype, and (3) adequate perfusion should minimize myocyte loss and the need for replacement fibrosis.

Global Transcriptional Changes in PVC-CM

The RNAseq data provided further evidence of extracellular matrix remodeling in PVC-CM by showing an upregulation of MMPs (3, 8, and 9), ADAMTS4, and ADAMTS9. These extracellular proteases can be secreted by fibroblasts, endothelial, and smooth muscle cells and are involved in extracellular matrix adaptations as part of many processes, such as development, fibrosis, and angiogenic responses.^{66–68} ADAMTS4 and MMP9 are secreted by cardiac fibroblasts^{69,70} and mediate the release of ECM-stored TGF (transforming growth factor)- β , which is an important pro-fibrotic factor.⁷¹ It was shown that the inhibition of ADAMTS4 prevents cardiac fibrosis in a model of pressure-overload in rats,⁷¹ while ADAMTS9 deficiency leads to heart abnormalities related to insufficient cleavage of versican,⁶⁸ a large extracellular matrix proteoglycan involved in cardiac fibrosis.⁷¹ Additionally, pro-fibrotic cytokines, such as IL-1 β and TGF- β , can upregulate MMPs expression

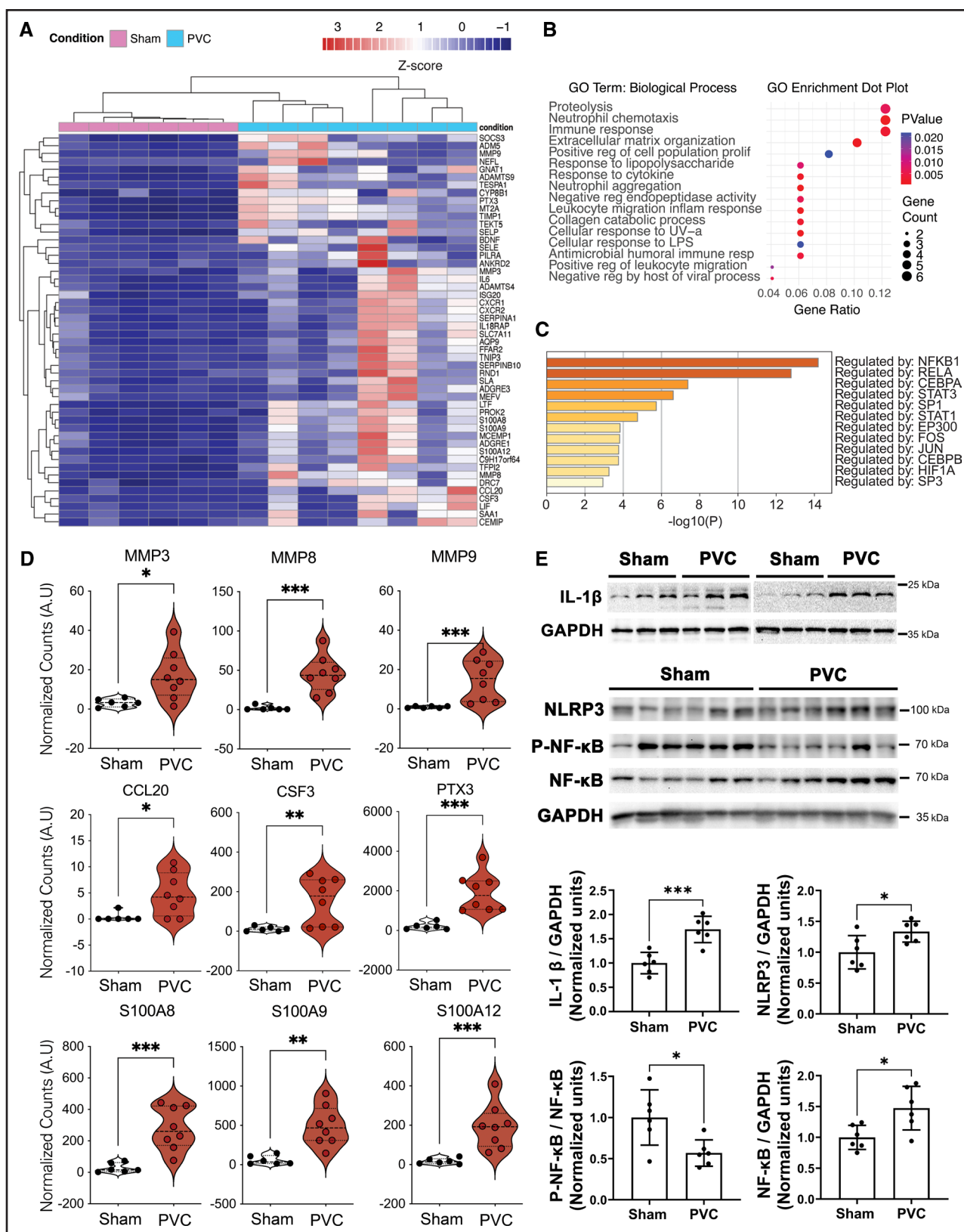


Figure 7. Premature ventricular contraction-induced cardiomyopathy (PVC-CM) results in a distinct transcription profile.

RNAseq was used to identify differentially transcribed genes. **A**, Heatmap displaying the top 50 upregulated genes. **B**, Gene set enrichment analysis of the top 50 upregulated genes. **C**, Enrichment for transcriptional regulatory networks identified from the transcriptional signature. **D**, Violin plots (marking 25th and 75th quartiles and median) showing transcripts of interest differentially expressed between groups. Nonparametric Mann-Whitney *U* test with 2-tailed was used for comparison between groups; *P* values are shown in (Continued)

Figure 7 Continued. asterisks * <0.05 , ** <0.01 , *** <0.001 . **E**, Western blot study showing protein expression in the LV tissue in PVC-CM with respect to sham: IL (interleukin)-1 β (** $P=0.007$ t test, n=6 animals per condition), NLRP3 (nucleotide-binding domain, leucine-rich repeat family, pyrin domain containing 3) (* $P=0.028$ t test, n=6 animals per condition), phospho-NF- κ B (nuclear factor kappa-light-chain-enhancer of activated B cells) p65 (Ser536; * $P=0.018$ t test, n=6 animals per condition), and total NF- κ B p65 (* $P=0.017$ t test, n=6 animals per condition). Bars are depicting mean \pm SD.

and activity in cardiac fibroblasts, promoting extracellular matrix remodeling.⁷² TIMP1, also elevated in PVC-CM, is an endogenous inhibitor of metalloproteinases, having a preference for MMP9.^{73–75} The complex interplay between MMPs and TIMPs dynamically controls the extracellular matrix homeostasis, where an increase in TIMP expression is associated with heart disease.⁷⁵

RNAseq experiments identified several transcripts linked to inflammatory responses in PVC-CM. Notably, transcripts such as CCL20, CSF3, and PTX3 were elevated by >9-fold. Cytokines, such as TGF- β and IL-1 β , activate the chemokine cascade, including CCL20, which further enhances the chemotaxis of immune cells and contributes to fibrosis^{76–78} and potentially to revascularization.⁷⁹ CSF3 is a key cytokine involved in neutrophil infiltration and promotes a profibrotic phenotype in the heart.⁸⁰ PTX3 acts as a regulator of the inflammatory response and tissue remodeling, including the differentiation of monocytes into fibrocytes, and its knockdown has been shown to decrease cardiac fibrosis.^{81,82} Additionally, PTX3 has been studied as a biomarker linked to an increased risk of cardiac events in patients with HF.⁸³ Several additional genes related to inflammation were upregulated in PVC-CM. SELE, which encodes E-selectin, is crucial for immune cell trafficking, as it facilitates the adhesion and transmigration of leukocytes into tissues.⁸⁴ Importantly, SELE is not constitutively expressed but is upregulated on the surface of endothelial cells in response to TNF- α or IL-1 β .⁸⁴ Other notable genes upregulated were CXCR1 and CXCR2, encoding C-X-C Motif Chemokine Receptors 1 and 2, respectively, both of which play a role in neutrophil recruitment.⁸⁵ The alarmins S100A8 and S100A9, abundantly stored in neutrophils as a heterodimer,⁸⁶ were also significantly upregulated in PVC-CM (Figure 7D). Cardiomyocytes also express S100A8/S100A9, which have been implicated in mitochondrial dysfunction and cardiomyocyte impairment in ischemia/reperfusion injury models.⁸⁷ These alarmins are also important mediators in the fibroblast-macrophage functional interaction leading to cardiac fibrotic remodeling.⁸⁸ S100A12 has been less studied in cardiovascular diseases, but together with S100A8/9 are considered as potential biomarkers for cardiac diseases.^{89,90} Collectively, the gene transcription profile observed in PVC-CM demonstrated a strong enrichment of the NF- κ B transcription factor network (Figure 7C). This network serves as a pivotal hub modulating immune responses and inflammation.^{91–94} Indeed, NF- κ B p65 (RelA) protein levels were elevated, while phosphorylation at the S536 residue was reduced in PVC-CM compared with sham (Figure 7E). As

phosphorylation at this site is known to attenuate inflammatory responses,^{95,96} these findings further support the role of NF- κ B as a mediator of the inflammatory transcriptomic response.

IL-1 β , a key cytokine at the interface of cardiac fibrosis and sterile inflammation predominantly produced by macrophages,^{33,97–100} was elevated in PVC-CM (Figure 7E). Likewise, the inflammasome component NLRP3 (critical for IL-1 β production) was increased in PVC-CM. Several actions of IL-1 β on the cardiac tissue described by others correlate with the phenotype observed in our PVC-CM model. For example, IL-1 β decreases L-type Ca²⁺ current,¹⁰¹ decreases SERCA expression, and reduces the amplitude of Ca²⁺ transients in ventricular myocytes.¹⁰² These effects of IL-1 β on Ca²⁺ handling are consistent with the phenotype previously described in our PVC-CM model.^{76,103} These associations support the new hypothesis that IL-1 β is an important mediator of the PVC-CM phenotype. Studies *in vivo* have shown that deletion of IL-1 β signaling decreases inflammatory and fibrotic responses in a model of myocardial infarction,^{37,104} arguing that elevated IL-1 β may also be involved in the pro-fibrotic effect observed in PVC-CM, a hypothesis that should be tested in future studies.

Consequently, the RNAseq data strongly indicate that an inflammatory response is associated with the adverse cardiac remodeling observed in PVC-CM, and the elevation of IL-1 β further supports this conclusion. This insight opens new avenues for future research into the underlying mechanisms of PVC-CM.

Study Limitations

In this study, a high burden of PVC of 50% (bigeminy) used in the experimental group is rarely observed in the clinical setting; however, it ensures that all animals will develop cardiomyopathy as previously published,¹⁰⁵ minimizing canine use in research. In this study, only female canines were used for experimentation. This is a limitation, since a number of clinical studies have identified sex as an independent predictor in the development of PVC-CM.^{2,5,106–109} Like in humans, frequent PVCs decrease the cardiac output with a tendency to produce a mild cardiomyopathy, and the severity of the ventricular dysfunction is proportional to the PVC burden.^{5,110} Similar to the clinical setting, eliminating PVCs results in the recovery of the ventricular function in a matter of weeks.⁹ Unfortunately, histological studies in human samples have not been reported, in part because the PVC-CM diagnosis can only be achieved after the LV

ejection fraction recovers on elimination of PVCs. Therefore, using this animal PVC-CM model is an effective alternative to perform these histopathologic studies in a systematic approach.

Although this large animal model is one of the best models to study PVC-CM, a significant limitation is the implementation of interventional molecular tools and genetic modifications. Therefore, this is mainly a comparative study, and cause-and-effect relationships must be further tested in simplified models that might lose translational value.

Clinical Implications

This study demonstrates that cardiac remodeling in PVC-CM is characterized by increased angiogenesis and capillary diameter, supporting the hypertrophic response. Transcriptional changes reveal an underlying aseptic inflammatory response, which, together with fibroblast proliferation and activation, leads to interstitial fibrosis. Reactive and interstitial fibrosis has been shown to affect electrophysiological properties that are likely associated with worse outcomes, as demonstrated by late gadolinium enhancement and extracellular volume assessed by cardiac MRI.^{46–48,111} Similar to tachycardia-induced cardiomyopathy,^{112,113} interstitial fibrosis in PVC-CM could result in increased risk of ventricular arrhythmias and mortality despite resolution of LV dysfunction after ablation of PVCs. A better understanding of the mechanisms driving inflammation and interstitial fibrosis in PVC-CM, as well as in other cardiomyopathies, could help to identify new therapies to prevent or minimize a persistent LV substrate associated with increased mortality and sudden cardiac death.

ARTICLE INFORMATION

Received June 25, 2025; accepted November 19, 2025.

Affiliations

Department of Cellular, Molecular and Genetic Medicine, School of Medicine (J.M.L.M.-C., J.B.-V., M.S., J.M.E.) and Pauley Heart Center (J.H., K.K., A.Y.T., J.F.H.), Virginia Commonwealth University, Richmond. Division of Pulmonary and Critical Care Medicine, University of Cincinnati, OH (J.G.-A.). Division of Cardiac Electrophysiology, Richmond Veterans Affairs Medical Center, VA (K.K., A.Y.T., J.F.H.).

Acknowledgments

Microscopy was performed at the VCU Department of Anatomy and Neurobiology Microscopy Facility. The graphic abstract was designed using BioRender (Dr Balderas-Villalobos [2025] <https://Biorender.com/mzbzk8d>).

Sources of Funding

This work was partially funded by National Institutes of Health (NIH), National Heart, Lung, and Blood Institute grant R01 HL139874 (Dr Huizar) and National Institute of Arthritis and Musculoskeletal and Skin Diseases R01 AR068431 (Dr Samsó), Department of Veterans Affairs grant 5I01BX004861 (Dr Huizar), Secretaría de Educación, Ciencia, Tecnología e Innovación de la Ciudad de México fellowship SECTEI/135/2019 (Dr Medina-Contreras) and a postdoctoral fellowship from the American Heart Association and the D.C. Women's Board 836430 (Dr Balderas-Villalobos). NIH Center core grant 5P30NS047463.

Disclosures

None.

Supplemental Material

Supplemental Methods
Tables S1 and S2
Figure S1

REFERENCES

- Kennedy HL, Whitlock JA, Sprague MK, Kennedy LJ, Buckingham TA, Goldberg RJ. Long-term follow-up of asymptomatic healthy subjects with frequent and complex ventricular ectopy. *N Engl J Med.* 1985;312:193–197. doi: 10.1056/NEJM198501243120401
- Huizar JF, Tan AY, Kaszala K, Ellenbogen KA. Clinical and translational insights on premature ventricular contractions and PVC-induced cardiomyopathy. *Prog Cardiovasc Dis.* 2021;66:17–27. doi: 10.1016/j.pcad.2021.04.001
- Baman TS, Lange DC, Ilg KJ, Gupta SK, Liu TY, Alguire C, Armstrong W, Good E, Chugh A, Jongnarangsin K, et al. Relationship between burden of premature ventricular complexes and left ventricular function. *Heart Rhythm.* 2010;7:865–869. doi: 10.1016/j.hrthm.2010.03.036
- Huizar JF, Ellenbogen KA. Is PVC-induced cardiomyopathy truly reversible? a deep dive into questions that remain unanswered. *JACC Clin Electrophysiol.* 2020;6:1377–1380. doi: 10.1016/j.jacep.2020.06.034
- Shoureshi P, Tan AY, Koneru J, Ellenbogen KA, Kaszala K, Huizar JF. Arrhythmia-induced cardiomyopathy: JACC state-of-the-art review. *J Am Coll Cardiol.* 2024;83:2214–2232. doi: 10.1016/j.jacc.2024.03.416
- Tan AY, Elharrif K, Cardona-Guarache R, Mankad P, Ayers O, Joslyn M, Das A, Kaszala K, Lin SF, Ellenbogen KA, et al. Persistent proarrhythmic neural remodeling despite recovery from premature ventricular contraction-induced cardiomyopathy. *J Am Coll Cardiol.* 2020;75:1–13. doi: 10.1016/j.jacc.2019.10.046
- Kowlgi GN, Tan AY, Kaszala K, Kontos MC, Lozano P, Ellenbogen KA, Huizar JF. Left ventricular dyssynchrony as marker of early dysfunction in premature ventricular contraction-induced cardiomyopathy. *Front Cardiovasc Med.* 2022;9:978341. doi: 10.3389/fcvn.2022.978341
- Torrado J, Kowlgi GN, Ramirez RJ, Balderas-Villalobos J, Jovin D, Parker C, Om E, Aripetov S, Kaszala K, Tan AY, et al. Eccentric hypertrophy in an animal model of mid- and long-term premature ventricular contraction-induced cardiomyopathy. *Heart Rhythm O2.* 2021;2:80–88. doi: 10.1016/j.hroo.2020.12.021
- Huizar JF, Kaszala K, Potfay J, Minisi AJ, Lesnfsky EJ, Abbate A, Mezzaroma E, Chen Q, Kukreja RC, Hoke NN, et al. Left ventricular systolic dysfunction induced by ventricular ectopy: a novel model for premature ventricular contraction-induced cardiomyopathy. *Circ Arrhythm Electrophysiol.* 2011;4:543–549. doi: 10.1161/CIRCEP.111.962381
- Tanaka Y, Rahmutula D, Duggirala S, Nazer B, Fang Q, Olgjin J, Sievers R, Gerstenfeld EP. Diffuse fibrosis leads to a decrease in unipolar voltage: validation in a swine model of premature ventricular contraction-induced cardiomyopathy. *Heart Rhythm.* 2016;13:547–554. doi: 10.1016/j.hrthm.2015.09.025
- Walters TE, Rahmutula D, Szilagyi J, Alheda C, Sievers R, Fang Q, Olgjin J, Gerstenfeld EP. Left ventricular dyssynchrony predicts the cardiomyopathy associated with premature ventricular contractions. *J Am Coll Cardiol.* 2018;72:2870–2882. doi: 10.1016/j.jacc.2018.09.059
- Qin M, Song ZL, Zhu XY, Zhang Y, Jiang WF, Wu SH, Shen XY, Liu T, Liu X. Temporal and spatial changes of proarrhythmic substrate in premature ventricular contraction-induced cardiomyopathy. *JACC Clin Electrophysiol.* 2023;9:173–188. doi: 10.1016/j.jacep.2022.09.026
- Shiojima I, Sato K, Izumiya Y, Schiekofer S, Ito M, Liao R, Colucci WS, Walsh K. Disruption of coordinated cardiac hypertrophy and angiogenesis contributes to the transition to heart failure. *J Clin Invest.* 2005;115:2108–2118. doi: 10.1172/JCI24682
- Sano M, Minamino T, Toko H, Miyauchi H, Orimo M, Qin Y, Akazawa H, Tateno K, Kayama Y, Harada M, et al. p53-induced inhibition of Hif-1 causes cardiac dysfunction during pressure overload. *Nature.* 2007;446:444–448. doi: 10.1038/nature05602
- Shimizu I, Minamino T. Physiological and pathological cardiac hypertrophy. *J Mol Cell Cardiol.* 2016;97:245–262. doi: 10.1016/j.yjmcc.2016.06.001
- White FC, Bloor CM, McKirnan MD, Carroll SM. Exercise training in swine promotes growth of arteriolar bed and capillary angiogenesis in heart. *J Appl Physiol (1985).* 1998;85:1160–1168. doi: 10.1152/jappl.1998.85.3.1160

17. Oldfield CJ, Duhamel TA, Dhalla NS. Mechanisms for the transition from physiological to pathological cardiac hypertrophy. *Can J Physiol Pharmacol.* 2020;98:74–84. doi: 10.1139/cjpp-2019-0566
18. Balderas-Villalobos J, Medina-Contreras JML, Lynch C, Kabadi R, Hayles J, Ramirez RJ, Tan AY, Kaszala K, Samso M, Huizar JF, et al. Mechanisms of adaptive hypertrophic cardiac remodeling in a large animal model of premature ventricular contraction-induced cardiomyopathy. *IUBMB Life.* 2023;75:926–940. doi: 10.1002/iub.2765
19. Bray NL, Pimentel H, Melsted P, Pachter L. Near-optimal probabilistic RNA-seq quantification. *Nat Biotechnol.* 2016;34:525–527. doi: 10.1038/nbt.3519
20. Soneson C, Love MI, Robinson MD. Differential analyses for RNA-seq: transcript-level estimates improve gene-level inferences. *F1000Res.* 2015;4:1521. doi: 10.12688/f1000research.7563.2
21. Love MI, Huber W, Anders S. Moderated estimation of fold change and dispersion for RNA-seq data with DESeq2. *Genome Biol.* 2014;15:550. doi: 10.1186/s13059-014-0550-8
22. Segnani C, Ippolito C, Antonioli L, Pellegrini C, Blandizzi C, Dolfi A, Bernardini N. Histochemical detection of collagen fibers by sirius red/fast green is more sensitive than van Gieson or sirius red alone in normal and inflamed rat colon. *PLoS One.* 2015;10:e0144630. doi: 10.1371/journal.pone.0144630
23. Sikkel MB, Francis DP, Howard J, Gordon F, Rowlands C, Peters NS, Lyon AR, Harding SE, MacLeod KT. Hierarchical statistical techniques are necessary to draw reliable conclusions from analysis of isolated cardiomyocyte studies. *Cardiovasc Res.* 2017;113:1743–1752. doi: 10.1093/cvr/cvx151
24. Eisner DA. Pseudoreplication in physiology: more means less. *J Gen Physiol.* 2021;153:e202012851. doi: 10.1085/jgp.202012851
25. Longden TA, Zhao G, Hariharan A, Lederer WJ. Pericytes and the control of blood flow in brain and heart. *Annu Rev Physiol.* 2023;85:137–164. doi: 10.1146/annurev-physiol-031522-034807
26. Su H, Cantrell AC, Zeng H, Zhu SH, Chen JX. Emerging role of pericytes and their secretome in the heart. *Cells.* 2021;10:548. doi: 10.3390/cells10030548
27. van Splunder H, Villacampa P, Martinez-Romero A, Graupera M. Pericytes in the disease spotlight. *Trends Cell Biol.* 2024;34:58–71. doi: 10.1016/j.tcb.2023.06.001
28. Gergely TG, Kovacs T, Kovacs A, Toth VE, Sayour NV, Morotz GM, Kovacs-Heszeli C, Brenner GB, Onodi Z, Enyedi B, et al. CardiLect: a combined cross-species lectin histochemistry protocol for the automated analysis of cardiac remodelling. *ESC Heart Fail.* 2025;12:1398–1415. doi: 10.1002/eihf.215155
29. Saljic A, Friederike Fenner M, Winters J, Flethoj M, Eggert Eggertsen C, Carstensen H, Dalgaard Nissen S, Melis Hesselkilde E, van Hunnik A, Schotten U, et al. Increased fibroblast accumulation in the equine heart following persistent atrial fibrillation. *Int J Cardiol Heart Vasc.* 2021;35:100842. doi: 10.1016/j.ijcha.2021.100842
30. Winters J, von Braunmuhl ME, Zeemering S, Gilbers M, Brink TT, Scaf B, Guasch E, Mont L, Batlle M, Sinner M, et al. JavaCyte, a novel open-source tool for automated quantification of key hallmarks of cardiac structural remodeling. *Sci Rep.* 2020;10:20074. doi: 10.1038/s41598-020-76932-3
31. Richardson WJ, Clarke SA, Quinn TA, Holmes JW. Physiological implications of myocardial scar structure. *Compr Physiol.* 2015;5:1877–1909. doi: 10.1002/cphy.c140067
32. Hinz B. Formation and function of the myofibroblast during tissue repair. *J Invest Dermatol.* 2007;127:526–537. doi: 10.1038/sj.jid.5700613
33. Frangogiannis NG. Cardiac fibrosis: Cell biological mechanisms, molecular pathways and therapeutic opportunities. *Mol Aspects Med.* 2019;65:70–99. doi: 10.1016/j.mam.2018.07.001
34. Kanisicak O, Khalil H, Ivey MJ, Karch J, Maliken BD, Correll RN, Brody MJ, J Lin SC, Aronow BJ, Tallquist MD, et al. Genetic lineage tracing defines myofibroblast origin and function in the injured heart. *Nat Commun.* 2016;7:12260. doi: 10.1038/ncomms12260
35. Manders EMM, Verbeek FJ, Aten JA. Measurement of co-localization of objects in dual-colour confocal images. *J Microsc.* 1993;169:375–382. doi: 10.1111/j.1365-2818.1993.tb03313.x
36. Saxena A, Chen W, Su Y, Rai V, Uche OU, Li N, Frangogiannis NG. IL-1 induces proinflammatory leukocyte infiltration and regulates fibroblast phenotype in the infarcted myocardium. *J Immunol.* 2013;191:4838–4848. doi: 10.4049/jimmunol.1300725
37. Bagheri SA, Hemmings KE, Yuldasheva NY, Maqbool A, Gamboa-Esteves FO, Humphreys NE, Jackson MS, Denton CP, Francis S, Porter KE, et al. Fibroblast-specific deletion of interleukin-1 receptor-1 reduces adverse cardiac remodeling following myocardial infarction. *JCI Insight.* 2019;5:e125074. doi: 10.1172/jci.insight.125074
38. Forstermann U, Boissel JP, Kleinert H. Expressional control of the ‘constitutive’ isoforms of nitric oxide synthase (NOS I and NOS III). *FASEB J.* 1998;12:773–790.
39. Li X, Lee C, Tang Z, Zhang F, Arjunan P, Li Y, Hou X, Kumar A, Dong L. VEGF-B: survival or an angiogenic factor? *Cell Adh Migr.* 2009;3:322–327. doi: 10.4161/cam.3.4.9459
40. Ge Q, Chen X, Zhao Y, Mu H, Zhang J. Modulatory mechanisms of NLRP3: potential roles in inflammasome activation. *Life Sci.* 2021;267:118918. doi: 10.1016/j.lfs.2020.118918
41. Torimoto K, Elliott K, Nakayama Y, Yanagisawa H, Eguchi S. Cardiac and perivascular myofibroblasts, matriffibrocytes, and immune fibrocytes in hypertension: commonalities and differences with other cardiovascular diseases. *Cardiovasc Res.* 2024;120:567–580. doi: 10.1093/cvr/cvae044
42. Francis Stuart SD, De Jesus NM, Lindsey ML, Ripplinger CM. The crossroads of inflammation, fibrosis, and arrhythmia following myocardial infarction. *J Mol Cell Cardiol.* 2016;91:114–122. doi: 10.1016/j.yjmcc.2015.12.024
43. Talman V, Ruskoaho H. Cardiac fibrosis in myocardial infarction—from repair and remodeling to regeneration. *Cell Tissue Res.* 2016;365:563–581. doi: 10.1007/s00441-016-2431-9
44. Cadour F, Quemeneur M, Biere L, Donal E, Bentatou Z, Eicher JC, Roubille F, Lalande A, Giorgi R, Rapacchi S, et al. Prognostic value of cardiovascular magnetic resonance T1 mapping and extracellular volume fraction in nonischemic dilated cardiomyopathy. *J Cardiovasc Magn Reson.* 2023;25:7. doi: 10.1186/s12968-023-00919-y
45. Jin C, Weber J, Singh H, Gliganic K, Cao JJ. Correction to: The association of reduced left ventricular strains with increased extracellular volume and their collective impact on clinical outcomes. *J Cardiovasc Magn Reson.* 2021;23:128. doi: 10.1186/s12968-021-00826-0
46. Jablonski R, Chaudry U, van der Pals J, Engblom H, Arheden H, Heiberg E, Wu KC, Borgquist R, Carlsson M. Cardiovascular magnetic resonance to predict appropriate implantable cardioverter defibrillator therapy in ischemic and nonischemic cardiomyopathy patients using late gadolinium enhancement border zone: comparison of four analysis methods. *Circ Cardiovasc Imaging.* 2017;10:e006105. doi: 10.1161/CIRCIMAGING.116.006105
47. Watanabe E, Abbasi SA, Heydari B, Coelho-Filho OR, Shah R, Neilan TG, Murthy VL, Mongeon FP, Barbhaiya C, Jerosch-Herold M, et al. Infarct tissue heterogeneity by contrast-enhanced magnetic resonance imaging is a novel predictor of mortality in patients with chronic coronary artery disease and left ventricular dysfunction. *Circ Cardiovasc Imaging.* 2014;7:887–894. doi: 10.1161/CIRCIMAGING.113.001293
48. Freitas P, Ferreira AM, Arteaga-Fernandez E, de Oliveira Antunes M, Mesquita J, Abecasis J, Marques H, Sarava C, Matos DN, Rodrigues R, et al. The amount of late gadolinium enhancement outperforms current guideline-recommended criteria in the identification of patients with hypertrophic cardiomyopathy at risk of sudden cardiac death. *J Cardiovasc Magn Reson.* 2019;21:50. doi: 10.1186/s12968-019-0561-4
49. Nerheim P, Birger-Botkin S, Piracha L, Olshansky B. Heart failure and sudden death in patients with tachycardia-induced cardiomyopathy and recurrent tachycardia. *Circulation.* 2004;110:247–252. doi: 10.1161/01.CIR.0000135472.28234.CC
50. Santulli G. *Angiogenesis: insights from a systematic overview.* Hauppauge New York: Nova Biomedical; 2013.
51. Verheule S, Schotten U. Electrophysiological consequences of cardiac fibrosis. *Cells.* 2021;10:3220. doi: 10.3390/cells10113220
52. Beenken A, Mohammadi M. The FGF family: biology, pathophysiology and therapy. *Nat Rev Drug Discov.* 2009;8:235–253. doi: 10.1038/nrd2792
53. Berthod F, Germain L, Tremblay N, Auger FA. Extracellular matrix deposition by fibroblasts is necessary to promote capillary-like tube formation in vitro. *J Cell Physiol.* 2006;207:491–498. doi: 10.1002/jcp.20584
54. Newman AC, Nakatsu MN, Chou W, Gershon PD, Hughes CC. The requirement for fibroblasts in angiogenesis: fibroblast-derived matrix proteins are essential for endothelial cell lumen formation. *Mol Biol Cell.* 2011;22:3791–3800. doi: 10.1091/mbc.E11-05-0393
55. Gogiraju R, Bochenek ML, Schafer K. Angiogenic endothelial cell signaling in cardiac hypertrophy and heart failure. *Front Cardiovasc Med.* 2019;6:20. doi: 10.3389/fcm.2019.00020
56. Giordano FJ, Gerber HP, Williams SP, VanBruggen N, Bunting S, Ruiz-Lozano P, Gu Y, Nath AK, Huang Y, Hickey R, et al. A cardiac myocyte vascular endothelial growth factor paracrine pathway is required to maintain cardiac function. *Proc Natl Acad Sci U S A.* 2001;98:5780–5785. doi: 10.1073/pnas.091415198

57. Yancopoulos GD, Davis S, Gale NW, Rudge JS, Wiegand SJ, Holash J. Vascular-specific growth factors and blood vessel formation. *Nature*. 2000;407:242–248. doi: 10.1038/35025215
58. Marneros AG. Effects of chronically increased VEGF-A on the aging heart. *FASEB J*. 2018;32:1550–1565. doi: 10.1096/fj.201700761RR
59. Zentilin L, Puligadda U, Lionetti V, Zacchigna S, Collesi C, Pattarini L, Ruozzi G, Camporesi S, Sinagra G, Pepe M, et al. Cardiomyocyte VEGFR-1 activation by VEGF-B induces compensatory hypertrophy and preserves cardiac function after myocardial infarction. *FASEB J*. 2010;24:1467–1478. doi: 10.1096/fj.09-143180
60. Wang Y, Eltis JM, Kaszala K, Tan A, Jiang M, Zhang M, Tseng GN, Huizar JF. Cellular mechanism of premature ventricular contraction-induced cardiomyopathy. *Heart Rhythm*. 2014;11:2064–2072. doi: 10.1016/j.hrthm.2014.07.022
61. Ito M, Shibata R, Ohashi K, Otaka N, Yamaguchi S, Ogawa H, Enomoto T, Masutomi T, Murohara T, Ouchi N. Omentin modulates chronic cardiac remodeling after myocardial infarction. *Circ Res*. 2023;5:46–54. doi: 10.1253/circres.CR-22-0079
62. Dai Z, Cheng J, Liu B, Yi D, Feng A, Wang T, An L, Gao C, Wang Y, Zhu MM, et al. Loss of endothelial hypoxia inducible factor-prolyl hydroxylase 2 induces cardiac hypertrophy and fibrosis. *J Am Heart Assoc*. 2021;10:e022077. doi: 10.1161/JAHA.121.022077
63. Li G, Gao J, Ding P, Gao Y. The role of endothelial cell-pericyte interactions in vascularization and diseases. *J Adv Res*. 2024;67:269–288. doi: 10.1016/j.jare.2024.01.016
64. Tomanek RJ. The coronary capillary bed and its role in blood flow and oxygen delivery: a review. *Anat Rec (Hoboken)*. 2022;305:3199–3211. doi: 10.1002/ar.24951
65. Kivela R, Bry M, Robciuc MR, Rasanen M, Taavitsainen M, Silvola JM, Saraste A, Hulmi JJ, Anisimov A, Mayranpaa MI, et al. VEGF-B-induced vascular growth leads to metabolic reprogramming and ischemia resistance in the heart. *EMBO Mol Med*. 2014;6:307–321. doi: 10.1002/emmm.201303147
66. Obika M, Vernon RB, Gooden MD, Braun KR, Chan CK, Wight TN. ADAMTS-4 and biglycan are expressed at high levels and co-localize to podosomes during endothelial cell tubulogenesis in vitro. *J Histochem Cytochem*. 2014;62:34–49. doi: 10.1369/0022155413507727
67. Santamaría S, de Groot R. ADAMTS proteases in cardiovascular physiology and disease. *Open Biol*. 2020;10:200333. doi: 10.1098/rsob.200333
68. Kern CB, Wessels A, McGarity J, Dixon LJ, Alston E, Argraves WS, Geeting D, Nelson CM, Menick DR, Apte SS. Reduced versican cleavage due to Adamts9 haploinsufficiency is associated with cardiac and aortic anomalies. *Matrix Biol*. 2010;29:304–316. doi: 10.1016/j.matbio.2010.01.005
69. Tucker NR, Chaffin M, Fleming SJ, Hall AW, Parsons VA, Bedi KC Jr, Akkad AD, Herndon CN, Arduini A, Papangeli I, et al. Transcriptional and cellular diversity of the human heart. *Circulation*. 2020;142:466–482. doi: 10.1161/CIRCULATIONAHA.119.045401
70. Yu Q, Stamenkovic I. Cell surface-localized matrix metalloproteinase-9 proteolytically activates TGF-beta and promotes tumor invasion and angiogenesis. *Genes Dev*. 2000;14:163–176.
71. Vistnes M, Erusappan PM, Sasi A, Norden ES, Bergo KK, Romaine A, Lunde IG, Zhang L, Olsen MB, Ogaard J, et al. Inhibition of the extracellular enzyme A disintegrin and metalloprotease with thrombospondin motif 4 prevents cardiac fibrosis and dysfunction. *Cardiovasc Res*. 2023;119:1915–1927. doi: 10.1093/cvr/cvad078
72. Li YY, McTiernan CF, Feldman AM. Interplay of matrix metalloproteinases, tissue inhibitors of metalloproteinases and their regulators in cardiac matrix remodeling. *Cardiovasc Res*. 2000;46:214–224. doi: 10.1016/s0008-6363(00)00003-1
73. Brew K, Dinakarpandian D, Nagase H. Tissue inhibitors of metalloproteinases: evolution, structure and function. *Biochim Biophys Acta*. 2000;1477:267–283. doi: 10.1016/s0167-4838(99)00279-4
74. Cabral-Pacheco GA, Garza-Veloz I, Castruita-De la Rosa C, Ramirez-Acuna JM, Perez-Romero BA, Guerrero-Rodriguez JF, Martinez-Avila N, Martinez-Fierro ML. The roles of matrix metalloproteinases and their inhibitors in human diseases. *Int J Mol Sci*. 2020;21:9739. doi: 10.3390/ijms21249739
75. Moore L, Fan D, Basu R, Kandalam V, Kassiri Z. Tissue inhibitor of metalloproteinases (TIMPs) in heart failure. *Heart Fail Rev*. 2012;17:693–706. doi: 10.1007/s10741-011-9266-y
76. Schutyser E, Struyf S, Van Damme J. The CC chemokine CCL20 and its receptor CCR6. *Cytokine Growth Factor Rev*. 2003;14:409–426. doi: 10.1016/s1359-6101(03)00049-2
77. Brand OJ, Somanath S, Moermans C, Yanagisawa H, Hashimoto M, Cambier S, Markovics J, Bondesson AJ, Hill A, Jablons D, et al. Transforming growth factor-beta and interleukin-1beta signaling pathways converge on the chemokine CCL20 promoter. *J Biol Chem*. 2015;290:14717–14728. doi: 10.1074/jbc.M114.630368
78. Yu M, Hu J, Zhu MX, Zhao T, Liang W, Wen S, Li HH, Long Q, Wang M, Guo HP, et al. Cardiac fibroblasts recruit Th17 cells infiltration into myocardium by secreting CCL20 in CVB3-induced acute viral myocarditis. *Cell Physiol Biochem*. 2013;32:1437–1450. doi: 10.1159/000356581
79. Lorchner H, Canes Esteve L, Goes ME, Harzenetter R, Brachmann N, Gajiwada P, Gunther S, Doll N, Poling J, Braun T. Neutrophils for revascularization require activation of CCR6 and CCL20 by TNFalpha. *Circ Res*. 2023;133:592–610. doi: 10.1161/CIRCRESAHA.123.323071
80. Jiang HM, Wang HX, Yang H, Zeng XJ, Tang CS, Du J, Li HH. Role for granulocyte colony stimulating factor in angiotensin II-induced neutrophil recruitment and cardiac fibrosis in mice. *Am J Hypertens*. 2013;26:1224–1233. doi: 10.1093/ajh/hpt095
81. Bottazzi B, Inforzato A, Messa M, Barbagallo M, Magrini E, Garlanda C, Mantovani A. The pentraxins PTX3 and SAP in innate immunity, regulation of inflammation and tissue remodelling. *J Hepatol*. 2016;64:1416–1427. doi: 10.1016/j.jhep.2016.02.029
82. Xu Y, Hu Y, Geng Y, Zhao N, Jia C, Song H, Bai W, Guo C, Wang L, Ni Y, et al. Pentraxin 3 depletion (PTX3 KD) inhibited myocardial fibrosis in heart failure after myocardial infarction. *Aging (Albany NY)*. 2022;14:4036–4049. doi: 10.18632/aging.204070
83. Suzuki S, Takeishi Y, Niizeki T, Koyama Y, Kitahara T, Sasaki T, Sagara M, Kubota I. Pentraxin 3, a new marker for vascular inflammation, predicts adverse clinical outcomes in patients with heart failure. *Am Heart J*. 2008;155:75–81. doi: 10.1016/j.ajh.2007.08.013
84. Zhang J, Huang S, Zhu Z, Gatt A, Liu J. E-selectin in vascular pathophysiology. *Front Immunol*. 2024;15:1401399. doi: 10.3389/fimmu.2024.1401399
85. Capucetti A, Albano F, Bonecchi R. Multiple roles for chemokines in neutrophil biology. *Front Immunol*. 2020;11:1259. doi: 10.3389/fimmu.2020.01259
86. Pruenster M, Vogl T, Roth J, Sperando M. S100A8/A9: from basic science to clinical application. *Pharmacol Ther*. 2016;167:120–131. doi: 10.1016/j.pharmthera.2016.07.015
87. Li Y, Chen B, Yang X, Zhang C, Jiao Y, Li P, Liu Y, Li Z, Qiao B, Bond Lau W, et al. S100a8/a9 signaling causes mitochondrial dysfunction and cardiomyocyte death in response to ischemic/reperfusion injury. *Circulation*. 2019;140:751–764. doi: 10.1161/CIRCULATIONAHA.118.039262
88. Liu J, Chen X, Zeng L, Zhang L, Wang F, Peng C, Huang X, Li S, Liu Y, Shou W, et al. Targeting S100A9 prevents beta-adrenergic activation-induced cardiac injury. *Inflammation*. 2024;47:789–806. doi: 10.1007/s10753-023-01944-w
89. Yu Y, Shi H, Wang Y, Yu Y, Chen R. A pilot study of S100A4, S100A8/A9, and S100A12 in dilated cardiomyopathy: novel biomarkers for diagnosis or prognosis? *ESC Heart Fail*. 2024;11:503–512. doi: 10.1002/ehf2.14605
90. Zhang Z, Ding J, Mi X, Lin Y, Li X, Lian J, Liu J, Qu L, Zhao B, Li X. Identification of common mechanisms and biomarkers of atrial fibrillation and heart failure based on machine learning. *ESC Heart Fail*. 2024;11:2323–2333. doi: 10.1002/ehf2.14799
91. Baeuerle PA, Baltimore D. NF-kappa B: ten years after. *Cell*. 1996;87:13–20. doi: 10.1016/s0092-8674(00)81318-5
92. Sha WC, Liou HC, Tuomanen EI, Baltimore D. Targeted disruption of the p50 subunit of NF-kappa B leads to multifocal defects in immune responses. *Cell*. 1995;80:321–330. doi: 10.1016/0092-8674(95)90415-8
93. Taniguchi K, Karin M. NF-kappaB, inflammation, immunity and cancer: coming of age. *Nat Rev Immunol*. 2018;18:309–324. doi: 10.1038/nri.2017.142
94. Matsumori A. Nuclear factor-kappaB is a prime candidate for the diagnosis and control of inflammatory cardiovascular disease. *Eur Cardiol*. 2023;18:e40. doi: 10.15420/ecr.2023.10
95. Pradere JP, Hernandez C, Koppe C, Friedman RA, Luedde T, Schwabe RF. Negative regulation of NF-kappaB p65 activity by serine 536 phosphorylation. *Sci Signal*. 2016;9:ra85. doi: 10.1126/scisignal.aab2820
96. Aoki T, Gao J, Li A, Huang F, Tu Y, Wu W, Matsuda M, Kyoshima T, Nishimura F, Jimi E. Phosphorylation of Serine 536 of p65(RelA) Downregulates Inflammatory Responses. *Inflammation*. 2025;48:1499–1512. doi: 10.1007/s10753-024-02140-0
97. Boza P, Ayala P, Vivar R, Humeres C, Caceres FT, Munoz C, Garcia L, Hermoso MA, Diaz-Araya G. Expression and function of toll-like receptor 4 and inflammasomes in cardiac fibroblasts and myofibroblasts: IL-1beta synthesis, secretion, and degradation. *Mol Immunol*. 2016;74:96–105. doi: 10.1016/j.molimm.2016.05.001

98. Torp MK, Yang K, Ranheim T, Huso Lauritzen K, Alfsnes K, Vinge LE, Aukrust P, Stensløkken KO, Yndestad A, Sandanger O. Mammalian target of rapamycin (mTOR) and the proteasome attenuates IL-1beta expression in primary mouse cardiac fibroblasts. *Front Immunol.* 2019;10:1285. doi: 10.3389/fimmu.2019.01285
99. Alfaidi M, Wilson H, Daigneault M, Burnett A, Ridger V, Chamberlain J, Francis S. Neutrophil elastase promotes interleukin-1beta secretion from human coronary endothelium. *J Biol Chem.* 2015;290:24067–24078. doi: 10.1074/jbc.M115.659029
100. Turner NA, Das A, Warburton P, O'Regan DJ, Ball SG, Porter KE. Interleukin-1alpha stimulates proinflammatory cytokine expression in human cardiac myofibroblasts. *Am J Physiol Heart Circ Physiol.* 2009;297:H1117–H1127. doi: 10.1152/ajpheart.00372.2009
101. El Khoury N, Mathieu S, Fiset C. Interleukin-1beta reduces L-type Ca²⁺ current through protein kinase C ϵ activation in mouse heart. *J Biol Chem.* 2014;289:21896–21908. doi: 10.1074/jbc.M114.549642
102. Combes A, Frye CS, Lemster BH, Brooks SS, Watkins SC, Feldman AM, McTiernan CF. Chronic exposure to interleukin 1beta induces a delayed and reversible alteration in excitation-contraction coupling of cultured cardiomyocytes. *Pflugers Arch.* 2002;445:246–256. doi: 10.1007/s00424-002-0921-y
103. Balderas-Villalobos J, Medina-Contreras JML, Lynch C, Kabadi R, Ramirez RJ, Tan AY, Kaszala K, Samso M, Huizar JF, Eltit JM. Alterations of sarcoplasmic reticulum-mediated Ca(2+) uptake in a model of premature ventricular contraction (PVC)-induced cardiomyopathy. *Mol Cell Biochem.* 2022;478:1447–1456. doi: 10.1007/s11010-022-04605-y
104. Bujak M, Dobaczewski M, Chatila K, Mendoza LH, Li N, Reddy A, Frangogiannis NG. Interleukin-1 receptor type I signaling critically regulates infarct healing and cardiac remodeling. *Am J Pathol.* 2008;173:57–67. doi: 10.2353/ajpath.2008.070974
105. Tan AY, Hu YL, Potfay J, Kaszala K, Howren M, Sima AP, Shultz M, Koneru JN, Ellenbogen KA, Huizar JF. Impact of ventricular ectopic burden in a premature ventricular contraction-induced cardiomyopathy animal model. *Heart Rhythm.* 2016;13:755–761. doi: 10.1016/j.hrthm.2015.11.016
106. Latchamsetty R, Yokokawa M, Morady F, Kim HM, Mathew S, Tilz R, Kuck KH, Nagashima K, Tedrow U, Stevenson WG, et al. Multicenter outcomes for catheter ablation of idiopathic premature ventricular complexes. *JACC Clin Electrophysiol.* 2015;1:116–123. doi: 10.1016/j.jacep.2015.04.005
107. Latchamsetty R, Bogun F. Premature ventricular complex-induced cardiomyopathy. *JACC Clin Electrophysiol.* 2019;5:537–550. doi: 10.1016/j.jacep.2019.03.013
108. Flore F, Lioncino M, Cicenia M, Garozzo D, Raimondo C, Di Mambro C, Silvetti MS, Drago F. Premature ventricular contraction-induced ventricular dysfunction in children without structural heart disease: a systematic review and meta-analysis. *Europace.* 2025;27:euaf167. doi: 10.1093/europace/euaf167
109. Attachapianich T, Thiravetyan B, Tribuddharat N, Jaroopipatkul S, Navaravong L. Premature ventricular contraction-induced cardiomyopathy: contemporary evidence from risk stratification, pathophysiology, and management. *J Clin Med.* 2024;13:2635. doi: 10.3390/jcm13092635
110. Takada H, Takeuchi S, Ando K, Kaito A, Yoshida S. Experimental studies on myocardial contractility and hemodynamics in extrasystoles. *Jpn Circ J.* 1970;34:419–430. doi: 10.1253/jcj.34.419
111. Yang EY, Ghosh MG, Khan MA, Gramze NL, Brunner G, Nabi F, Nambi V, Nagueh SF, Nguyen DT, Graviss EA, et al. Myocardial extracellular volume fraction adds prognostic information beyond myocardial replacement fibrosis. *Circ Cardiovasc Imaging.* 2019;12:e009535. doi: 10.1161/CIRCIMAGING.119.009535
112. Hasdemir C, Yuksel A, Camli D, Kartal Y, Simsek E, Musayev O, Isayev E, Aydin M, Can LH. Late gadolinium enhancement CMR in patients with tachycardia-induced cardiomyopathy caused by idiopathic ventricular arrhythmias. *Pacing Clin Electrophysiol.* 2012;35:465–470. doi: 10.1111/j.1540-8159.2011.03324.x
113. Ling LH, Kalman JM, Ellims AH, Iles LM, Medi C, Sherratt C, Kaye DM, Hare JL, Kistler PM, Taylor AJ. Diffuse ventricular fibrosis is a late outcome of tachycardia-mediated cardiomyopathy after successful ablation. *Circ Arrhythm Electrophysiol.* 2013;6:697–704. doi: 10.1161/CIRCEP.113.000681